NON-ENZYMATIC FLUORESCENCE SENSOR BASED ON SILICON QUANTUM DOTS IN DETECTING URIC ACID AND GLUCOSE

By

GREMA HASSAN

© COPYRIGHT UPM

Thesis Submitted to the School of Graduate Studies, Universiti Putra Malaysia, in Fulfilment of the Requirements for the Degree of Master of Science

November 2024

FS 2024 20

All material contained within the thesis, including without limitation text, logos, icons, photographs and all other artwork, is copyright material of Universiti Putra Malaysia unless otherwise stated. Use may be made of any material contained within the thesis for non-commercial purposes from the copyright holder. Commercial use of the material may only be made with the express, prior, written permission of Universiti Putra Malaysia.

Copyright © Universiti Putra Malaysia

© COPYRIGHT UPM

Abstract of thesis presented to the Senate of Universiti Putra Malaysia in fulfilment of the requirement for the degree of Master of Science

NON-ENZYMATIC FLUORESCENCE SENSOR BASED ON SILICON QUANTUM DOTS IN DETECTING URIC ACID AND GLUCOSE

By

GREMA HASSAN

November 2024

Chairman : Associate Professor Jaafar bin Abdullah, PhD
Faculty : Science

Recent interest has focused on developing nanomaterials with diverse properties with silicon quantum dots (SiQDs) emerging as a leading candidate due to their excellent optical features, biocompatibility, chemical photostability, and water solubility. This study presents the synthesis and application of fluorescence-based SiQDs for the detection of uric acid and glucose, two important biomarkers for monitoring metabolic diseases. SiQDs were synthesized via a one-pot hydrothermal process, using 3-aminopropyltriethoxysilane (APTES) as a precursor, trisodium citrate as a reducing agent, and ethylenediamine as a capping agent. The optical properties of the SiQDs were characterized by UV-Vis and fluorescence spectroscopy, revealing an absorption range of 200–400 nm with a peak at 329 nm and maximum emission at 382 nm (excitation at 305 nm). Fourier Transmission Infrared (FTIR) analysis confirmed successful surface functionalization, showing Si–O bending vibrations at 1101 cm^{-1} and 1001 cm^{-1}. High-resolution transmission Electron Microscopy (HRTEM) analysis showed a uniform, near-spherical morphology, with sizes ranging from 11.81 to 12.95 nm, while X-ray diffraction (XRD) indicated an amorphous structure. For uric acid,

© COPYRIGHT UPM

fluorescence quenching due to SiQD self-aggregation allowed for detection in the range of 0.004 to 0.100 mg/ml, with a regression equation of y=23346x+3599.2 (R^2=0.980), a limit of detection (LOD) of 0.003 mg/ml, and a limit of quantification (LQD) of 0.061 mg/ml. In the case of glucose detection, the SiQDs exhibited linearity in the concentration range of 0.1 to 0.8 mg/ml, with a regression equation of y=20249x−1682.4 (R^2=0.9804), a LOD of 0.031 mg/ml, and LQD of 0.09 mg/ml. These results demonstrate that SiQDs offer a sensitive, reliable, and promising platform for the optical detection of glucose and uric acid, with potential applications in disease diagnosis and healthcare monitoring.

Keyword: Fluorescence, Non-Enzymatic, Quantum Dots, Quenching

SDG: GOAL 3: Good Health and Well-Being, GOAL 9: Industry, Innovation and Infrastructure

© COPYRIGHT UPM

Abstrak tesis yang dikemukakan kepada Senat Universiti Putra Malaysia sebagai memenuhi keperluan untuk ijazah Master Sains

SENSOR PENDARFLUOR BUKAN ENZIMATIK BERASASKAN TITIK KUANTUM SILIKON DALAM MENGESAN ASID URIK DAN GLUKOSA

Oleh

GREMA HASSAN

November 2024

Pengerusi : Profesor Madya Jaafar bin Abdullah, PhD
Fakulti : Sains

Kebelakangan ini minat pada pembangunan bahan nano dengan sifat yang pelbagai dengan titik kuantum silikon (SiQDs) muncul sebagai calon utama kerana ciri optikal yang sangat baik, keserasianbio, kestabilan foto kimia dan keterlarutan air. Kajian ini membentangkan sintesis dan aplikasi SiQDs berasaskan pendarfluor untuk pengesanan asid urik dan glukosa, dua biopenanda penting untuk memantau penyakit metabolik. SiQDs telah disintesis melalui proses hidroterma satu periuk, menggunakan 3-aminopropiltrietoksisilana (APTES) sebagai bahan pemula, trisodium sitrat sebagai agen penurunan, dan etilendiamina sebagai agen penyekat. Sifat optik SiQDs dicirikan oleh spektroskopi UV-Vis dan pendarfluor, menunjukkan julat penyerapan 200-400 nm dengan puncak pada 329 nm dan pancaran maksimum pada 382 nm (pengujaan pada 305 nm). Analisis Transmisi Fourier Inframerah (FTIR) mengesahkan kefungsian permukaan berjaya, menunjukkan getaran lentur Si–O pada 1101 cm^{-1} dan 1001 cm^{-1}. Analisis Mikroskopi Transmisi Elektron Resolusi Tinggi (HRTEM) menunjukkan morfologi hampir sfera seragam, dengan saiz antara 11.81 hingga 12.95 nm, manakala Pembelauan sinar-X (XRD) menunjukkan struktur amorfus. Untuk asid

© COPYRIGHT UPM

urik, pelindapan pendarfluor disebabkan oleh pengagregatan kendiri SiQDs berlaku untuk pengesanan dalam julat 0.004 hingga 0.100 mg/ml, dengan persamaan regresi y=23346x + 3599.2 (R2 = 0.980), had pengesanan (LOD) sebanyak 0.003 mg/ml, dan had kuantifikasi (LQD) sebanyak 0.061 mg/ml. Dalam kes pengesanan glukosa, SiQDs mempamerkan kelinearan dalam julat kepekatan 0.1 hingga 0.8 mg/ml, dengan persamaan regresi y=20249x−1682.4 (R^2 = 0.9804), LOD 0.031 mg/ml, dan LOQ sebanyak 0.09 mg/ml. Keputusan ini menunjukkan bahawa SiQDs menawarkan platform yang sensitif, boleh dipercayai dan menjanjikan pengesanan optik glukosa dan asid urik, dengan aplikasi yang berpotensi dalam diagnosis penyakit dan pemantauan penjagaan kesihatan.

Kata kunci: Bukan Enzimatik, Pelindapan, Pendarfluor, Titik Kuantum.

SDG: MATLAMAT 3: Kesihatan dan Kesejahteraan Yang Baik, MATLAMAT 9: Industri, Inovasi dan Infrastruktur

© COPYRIGHT UPM

ACKNOWLEDGMENTS

Above all, I offer my deepest praise and gratitude to Allah S.W.T. Without His blessings, I am nothing. He has provided me with everything I need in life, granting me the strength, wisdom, and perseverance to complete this study.

I would like to express my sincere appreciation to my supervisor, Assoc. Prof. Dr. Jaafar Abdullah, for his invaluable guidance and unwavering support throughout my research journey. Your advice and encouragement have been truly instrumental, and I am deeply grateful for your assistance whenever I sought it.

My heartfelt thanks also go to my co-supervisor, Prof. Nor Azah Yusof, for her generous support—not only in conducting this research but also throughout my coursework.

I am profoundly grateful to the Tertiary Education Trust Fund (TETFUND) and my institution, Ramat Polytechnic, Maiduguri, for their financial support and encouragement, which made this research possible.

Lastly, I owe an immeasurable debt of gratitude to my mother, my wife, and my children for their sacrifices, unwavering support, and constant prayers. Words cannot fully express my appreciation for all they have done.

© COPYRIGHT UPM

This thesis was submitted to the Senate of Universiti Putra Malaysia and has been accepted as fulfilment of the requirement for the degree of Master of Science. The members of the Supervisory Committee were as follows:

Jaafar bin Abdullah, PhD
Associate Professor
Faculty of Science
Universiti Putra Malaysia
(Chairman)

Nor Azah binti Yusof, PhD
Professor
Faculty of Science
Universiti Putra Malaysia
(Member)

ZALILAH MOHD SHARIFF, PhD
Professor and Dean
School of Graduate Studies
Universiti Putra Malaysia

Date: 8 May 2025

© COPYRIGHT UPM

TABLE OF CONTENTS

© COPYRIGHT UPM

© COPYRIGHT UPM

LIST OF TABLES

© COPYRIGHT UPM

LIST OF FIGURES

© COPYRIGHT UPM

© COPYRIGHT UPM

LIST OF ABBREVIATIONS

AA	Ascorbic Acid
APTES	3-Aminopropyl triethoxysilane
APTMS	3-[2-(2-aminoethyl amino) ethylamine]Propyl trimethoxysilane
ATP	Adenosine Triphosphate
BSA	Bovine Serum Albumin
CGA	Chlorogenic Acid
DAMO	N-[3-(trimethoxysilyl)]-ethylenediamine
DAP	2,3 - Diamino phenazine
DNA	Adenine Dinucleotide
EDA	Ethylene diamine
FAD	Flavin Adenine Dinucleotide Drugs
FRET	Fluorescence Resonance Energy Transfer
FRET	Foster resonance Energy Transfer
FTIR	Fourier Transmission infra-red
HFCS	High-Fructose Corn syrup
HPLC	High Power Liquid Chromatography
HRTEM	High Resolution Transmission Electron Microscope
IDF	International Diabetic Federation
IFE	Inner Filter Effect
LDH	Lactate Dehydrogenase
MEF	Metal-Enhanced Fluorescence
NADH	Nicotinamide Adenine Dinucleotide
NP	Nano Particles
ODP	O – Phenylene diamine

© COPYRIGHT UPM

OTC	Oxytetracycline
PET	Photo-Induced Electron Transfer
PL	Photoluminescence
QDS	Quantum Dots
QDS	Surface Plasmon Resonance
RSD	Relative Standard Deviation
SD	Standard Deviation
SERS	Surface -Enhanced Raman Spectroscopy
SET	Surface Energy Transfer
SiNDs	Silicon nanodots
SiNP	Silicon Nano Particles
SiQDs	Silicon Quantum Dots
T2D	Type 2 Diabetes
UPTES	Urea Propyltriethoxysilane
UV	Ultra -Violet
XRD	X-Ray Diffraction

© COPYRIGHT UPM

CHAPTER 1

INTRODUCTION

1.1 Background of the study

Uric acid ($C_6H_4N_4O_3$) is a substance that results from the breakdown of purine derivatives during human metabolism. Several tissues in the body, such as the liver, intestines, endothelium, muscles, and kidneys, produce uric acid. The kidneys mainly remove uric acid. Since humans lack the uricase enzyme, uric acid cannot be converted into a more water-soluble form, ending up in the urine. (El Ridi & Tallima, 2017). The kidneys reabsorb around 90% of the filtered uric acid back into the body, underscoring its essential physiological role. Uric acid also plays a significant role as an antioxidant, contributing to over 50% of the plasma's antioxidant activity (Baig et al., 2022).

Gout happens when a person has extremely high amounts of uric acid in their blood and urine. Through the elimination of soluble uric acid, the kidneys are crucial for blood purification. Health problems like kidney stones, diabetes, heart failure, gout, high blood pressure, and high cholesterol can all be brought on by an excess of uric acid (Bobulescu & Moe, 2012). Conversely, insufficient uric acid in the bloodstream can contribute to atherosclerosis and stroke, underscoring the importance of regulating uric acid levels for overall well-being. In men, the normal range of uric acid in the bloodstream is typically between 3.5 and 7.2 mg/dL, while in women, it ranges between 2.6 and 6 mg/dL (Yaacob et al., 2022). In contrast, uric acid in urine is usually higher than in blood, ranging from 25 to 74 mg/dL. Monitoring and maintaining

© COPYRIGHT UPM

optimum uric acid concentrations is essential to protect human health (Yaacob et al., 2020). Gout, a type of inflammatory arthritis, has a prevalence that varies across regions and populations, affecting an estimated 1% to 4% of adults globally, or approximately 75 to 300 million people. It is more common among older adults, individuals with obesity, and those with a family history of the condition (Dehlin et al., 2020). Studies from North America and Scandinavia indicate that gout prevalence has increased by 1.5 to 2 times in recent decades, while the Global Burden of Disease study found that gout incidence doubled between 1990 and 2017, reflecting similar trends worldwide. In Canada, gout-related hospitalizations and inpatient medical costs doubled between 2000 and 2011, and comparable patterns have been observed in Aotearoa New Zealand, the United Kingdom and Spain. However, the actual number of gout cases may be higher due to significant under reporting in medical records (Sivera et al., 2022).

Glucose, the most common carbohydrate and organic compound (considering all its forms), is a monosaccharide type, a simple sugar. Also known as dextrose, it is found in fruits and honey and is the main sugar present in the blood of higher animals. (Shendurse & Khedkar, 2021). Glucose is likely one of the most essential biological compounds in nature. It serves as the main energy source for glycolysis and subsequent anaerobic and aerobic respiration processes, providing the energy needed for growth and reproduction. (Galant et al., 2020). According to the International Diabetes Federation (IDF), approximately 537 million adults (ages 20-79) were living with diabetes in 2021, and this number is projected to rise to 783 million by 2045. Type 2 diabetes, which accounts for 90-95% of cases, is often linked to lifestyle factors (Sun et al., 2022). Glucose detection is critical in life sciences, biology, clinical diagnostics,

© COPYRIGHT UPM

and the food industry. The growing prevalence of diabetes, predicted to reach 642 million by 2030, underscores its impact as a global health crisis and its potential to become the 7th leading cause of death (Feng et al., 2021; Solanki et al., 2021).

Glucose, often referred to as dextrose, is a simple monosaccharide and the most prevalent carbohydrate and organic compound, primarily found in fruits and honey. It is a crucial energy source for glycolysis and both anaerobic and aerobic respiration, making it one of nature's most essential biological compounds for growth and reproduction. (Shendurse & Khedkar, 2021; Galant et al., 2020).

Glucose is commonly found in significant amounts in fruits, milk, and their derivatives, alongside other sugars such as fructose and sucrose. Cane juice contains sucrose, along with small amounts of glucose and fructose. If glucose and fructose levels increase, it indicates that sucrose is breaking down. Monitoring these sugars during processing in sugar factories is important for maintaining quality and reducing losses. (Mohamed & Higazi, 2016). Plants create sugars through photosynthesis, storing them as starch or converting them into disaccharides like sucrose. Sugars serve as a primary energy source for living organisms, with herbivores relying on these sugars for energy. However, humans tend to consume excessive refined sugar, far exceeding what the body can handle. This excessive intake contributes to health problems such as weight gain, heart disease, diabetes, high blood pressure, and dental issues. Therefore, it is essential to be mindful of the sugar content in foods and beverages (Ramasami et al., 2004). Determining glucose levels in food is crucial for monitoring nutritional content, particularly for individuals managing conditions like diabetes, where blood sugar regulation is critical. It helps manufacturers ensure

© COPYRIGHT UPM

product consistency and quality while enabling consumers to make informed dietary choices. Additionally, measuring glucose is important for understanding the carbohydrate composition of foods, which impacts energy content and overall health (Rambla et al., 2023).

1.2 Problem statement

Gout and diabetes are health problems that need ongoing attention and affect many people. People with these conditions usually get prescribed medications and have regular tests to check their uric acid and glucose levels. It's important to consistently monitor these levels to effectively evaluate their health (Upadhyay et al., 2022). Detecting one's health status in the early stages through prompt medical screening is highly crucial. A broad range of health screening methods exists, including dual electrochemical sensors for glucose/uric acid (Guo & Ma, 2017), smartphone as an electrochemical analyser (Guo, 2016), calorimetric detection (Nishan et al., 2022), microfluidic paper for glucose and uric acid (Yu et al., 2021), from self-monitoring to assessments conducted by healthcare experts. These procedures can be categorized as either invasive or non-invasive. Invasive approaches often entail pricking the fingertip to draw blood, occasionally resulting in calluses, scarring, and discomfort. Alternative body fluids like saliva, sweat, urine, or tears can be used as non-invasive means for healthcare monitoring because they frequently carry disease-related biomarkers in an easy-to-read manner. These fluids reduce the disadvantage of drawing blood during medical examinations (Azmi et al., 2018).

© COPYRIGHT UPM

Many methods have been reported for the analysis of uric acid and glucose, including fluorescence analysis (Wang et al., 2018), electrochemical assessment (Tukimin et al., 2017), HPLC-UV detection (Pleskacova et al., 2017), surface-enhanced Raman scattering, and enzymatic-UV detection (Westley et al., 2017). Of these, fluorescence analysis is regarded as the most effective approach for detecting uric acid and glucose due to its uncomplicated procedure, swift outcomes, heightened sensitivity, and economical nature. However, many fluorescence-based approaches necessitate the presence of uricase and glucose oxidase to scrutinize the distinct substances generated by their respective catalytic reactions. As enzymes are both delicate and costly, developing robust and cost-effective non-enzymatic fluorescence techniques is important in uric acid and glucose detection (Zheng et al., 2021).

Separate assays must be used to detect uric acid and glucose. Numerous detection techniques exist, but they might not be able to analyse numerous metabolites from a solitary sample simultaneously. Moreover, there's a notable requirement for compact, affordable, and user-friendly portable devices to facilitate effective monitoring of metabolites (Gao et al., 2019).

Due to their favourable properties, silicon quantum dots (SiQDs), a novel class of photoluminescent nanoparticles, have recently attracted the attention of researchers. Silicon quantum dots have excellent characteristics such as high water solubility, minimal toxicity, persistent photoluminescence, great biocompatibility, and a broad absorption spectrum. Due to these qualities, silicon quantum dots are in high demand for applications requiring fluorescence imaging and detection. Studies in the literature indicate that these quantum dots are commonly synthesized using electrochemical

© COPYRIGHT UPM

(Morozova et al., 2020), hydrothermal (Chen et al., 2018; Zhou et al., 2022; Liu et al., 2022), ultraviolet irradiation (Li, et al., 2020; J. Wu et al., 2015) and microwave techniques (Li et al., 2021; Xuan et al., 2014) either in their original form or after suitable modifications. These methods can produce quantum dots in their natural state or change them to meet certain requirements (Eda et al., 2020). A straightforward, safe, cost-effective, water-soluble substance with excellent biocompatibility and intense photoluminescence is available. Silicon quantum dots can be synthesized by a hydrothermal technique to quantitatively detect uric acid in urine and glucose in food samples.

1.3 Research Objectives

This study aims to develop an inexpensive, highly reliable, and fluorescence-based optical device derived from silicon quantum dots to detect uric acid and glucose. The following precise goals will be addressed to reach the study's goal:

i. To synthesize silicon quantum dots using 3-aminopropyl triethoxysilane (APTES) as the silicon source, ethylene diamine (EDA) as the capping agent, and sodium citrate as a reducing agent through the hydrothermal technique.

ii. To characterise the synthesised silicon quantum dots using optical techniques such as UV-visible spectroscopy, fluorescence spectroscopy, and FTIR, as well as structural analysis methods like HRTEM and XRD.

iii. To evaluate the performance of the synthesised silicon quantum dots in detecting uric acid and glucose in aqueous samples.

1.4 Significance of study

Biomarkers like uric acid can provide valuable insights into diabetes and gout. Optical sensors can enhance painless, non-invasive monitoring of biomarker levels, improving

© COPYRIGHT UPM

patient comfort and compliance. Glucose in food plays a crucial role in dietary management, especially for individuals with conditions like diabetes. Optical sensors for glucose detection can improve food quality control and provide consumers with accurate information, helping them make healthier choices and manage their blood sugar levels more effectively.

Silicon quantum dots exhibit unique optical properties, enhancing sensor sensitivity and specificity. Silicon quantum dots contribute to medical sensor reliability and extend detection possibilities beyond uric acid. Determination of glucose in food using silicon quantum dots-based sensors allows for precise and rapid analysis, ensuring better quality control in the food industry. This technology aids in monitoring glucose content in various products, offering valuable data for health-conscious consumers and individuals managing conditions like diabetes.

1.5 Scope and limitation

The research aims to create an optical sensor using silicon quantum dots for detecting uric acid and glucose. The study will assess the sensor's framework, sensitivity, precision, and accuracy, testing it with different biomarker concentrations. To quantify changes in the optical properties of the quantum dots, techniques like fluorescence, and absorbance will be used.

The limitations of this research involve synthesizing silicone Quantum Dots via a hydrothermal method to obtain a narrow size distribution is difficult, and a broad size distribution can result in a broad emission spectrum, reducing the sensor’s spectral

© COPYRIGHT UPM

resolution and specificity. The other challenging in the use of silicon quantum dots to quantitatively detect uric acid in urine samples and glucose in food samples which involve selectivity and sensitivity.

© COPYRIGHT UPM

CHAPTER 2

LITERATURE REVIEW

2.1 Uric acid and Glucose

Uric acid (Figure 2.1), a crucial by-product of purine breakdown in our bodies, is excreted through urine. Excessive uric acid, resulting from purine metabolism, has been proven to contribute to the initiation and progression of certain diseases. Elevated blood uric acid levels are directly correlated with the severity and advancement of these diseases. This naturally occurring substance, composed of carbon, nitrogen, oxygen, and hydrogen can lead to various health conditions when present at elevated levels. These conditions include gout, Lesh-Nyhan syndrome, hyperuricemia, kidney stones, physical ailments, high blood pressure, and renal disease (Saidin et al., 2018; Nishan et al., 2022).

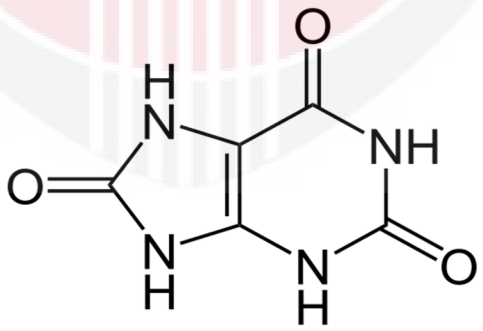

Figure 2.1: Structural formula of uric acid

A naturally existing compound that plays an important role in sustaining life is called glucose, ($C_6H_{12}O_6$). It serves as a primary source of energy for glycolysis and is

© COPYRIGHT UPM

intricately involved in both aerobic and anaerobic respiration processes. In clinical settings, glucose is employed for diagnosing diabetes, a metabolic disorder posing a substantial global health challenge. Individual with diabetes, either produce insulin or cannot effectively utilize the insulin their body generates. The World Health Organization reports that roughly three hundred and forty-seven million people globally have diabetes, with more than eighty percent of cases found in less affluent nations. Additionally, in 2012, it was estimated that diabetes directly resulted in 1 million five hundred thousand deaths positioning it as the 7th most common contributor to death by 2030 (Witkowska Nery, 2016). Diabetes increases the risk of heart disease and stroke, as well as foot ulcers that, when combined with infections, can lead to limb amputation. It also contributes to retinopathy, leading to vision loss, and kidney failure (Ahmad, 2017).

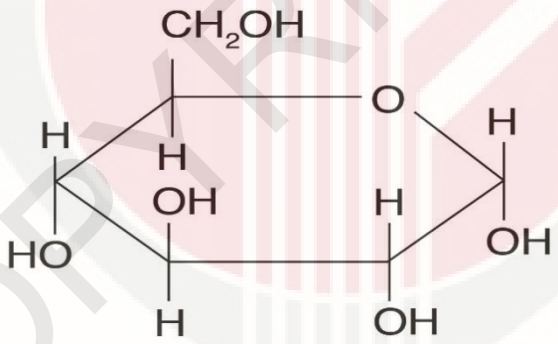

Figure 2.2: Structure of Glucose

Controlling uric acid is crucial for maintaining cardiovascular health, as insufficient levels may increase the risk of atherosclerosis and stroke. There are two ways to monitor uric acid levels: through plasma tests and urine tests. It's important to note that the healthy range of uric acid in urine is higher than that in the blood, typically ranging from 25 – 74 mg/dL (Yaacob et al., 2020)**.** Recently, there has been significant research

© COPYRIGHT UPM

into various analytical methods for detecting uric acid in human urine, including electro-analytical, luminescence, chromatography, and spectroscopy techniques (Tukimin et al., 2017). At the same time, measuring glucose and uric acid in urine is clinically important. Glucose levels can indicate conditions like diabetes, alcohol consumption, obesity, and high cholesterol. On the other hand, uric acid levels can signal gout, high blood pressure, kidney disease, heart disease, and related health issues (Yu et al., 2021).

2.2 Relationship between gout and diabetes

Gout is when uric acid crystals accumulate in the joints, leading to painful and recurring arthritis attacks. The rates of hyperuricemia and gout have risen recently, possibly due to environmental factors. Lifestyle and diet are linked to these conditions, with factors such as high body weight, alcohol consumption, and excessive meat and seafood intake being involved. Recent studies also suggest that consuming too much fructose may contribute to hyperuricemia and gout (Jamnik et al., 2022). Fructose is a simple sugar commonly found in plants and is a key ingredient in sugar-sweetened drinks. Studies show that the rise in hyperuricemia (high uric acid) and gout in developed countries matches the increase in fructose and high-fructose corn syrup (HFCS) consumption. Unlike glucose, fructose uses up ATP during processing in the body, which can raise uric acid levels (Jamnik et al., 2022).

Consumption of too much sugar can cause metabolic problems, leading to high blood sugar, insulin resistance, and fat gain. In obese people, high sugar intake increases urate levels and reduces the removal of uric acid, showing a strong link between high

© COPYRIGHT UPM

uric acid levels and a sugary diet(Zhang et al., 2022). Sugar-sweetened beverages, which contain high-fructose corn syrup, sucrose, or nearly equal amounts of fructose and glucose, make up about one-third of the added sugar consumed by American adults. These drinks are believed to be strongly linked to the high rates of hyperuricemia seen in Western countries (Chevinsky et al., 2021). The increased consumption of fructose-containing drinks, foods, and table sugar (sucrose) over the past centuries has contributed to weight gain, fat build-up in the liver and abdomen, insulin resistance, and a rise in diabetes. It has also led to higher uric acid levels, which increase the risk of metabolic syndrome and diabetes (El Ridi & Tallima, 2017).

2.3 Urine as a biomarker

Urine samples exhibit a rich biological diversity, containing various substances such as urea, amino acids, chlorides, potassium, phosphates, sodium, sulphates, and other trace chemicals. Obtaining urine samples is a straightforward process. Moreover, the average human produces a considerable daily amount of urine, ranging from 400 to 2000 ml. This makes urine an ideal non-invasive sample to detect biomarkers (Lepowsky et al., 2017). For example, excessive calcium and urine oxalate levels may indicate kidney stones (Orramongkona et al., 2018), while high protein and urine glucose levels could indicate diabetes (Fava et al., 2019). Similarly to this, increased urine serotonin levels can be a sign of melancholy (Roychoudhury et al., 2020).

The quantity of fluids a person drinks throughout the day is closely linked to how much urine they produce, which is why this is often discussed when evaluating patients with excessive urination (polyuria). However, the diuretic effects of different beverages and

© COPYRIGHT UPM

the impact of food intake are frequently overlooked. Food can contribute up to 20% of daily water intake through water content. Additionally, urine volume is influenced by how the kidneys process and concentrate waste from nutrients and minerals found in food. Certain foods may also have a diuretic effect, as recognized in traditional medicine, where they have been used to treat conditions like swelling, high blood pressure, and urinary issues (Alwis et al., 2020).

2.4 Food as a source of glucose

Functional foods offer health benefits beyond basic nutrition, often aiding in disease prevention or management. Despite containing antinutrients like phytic acid or trypsin inhibitors, they still contribute positively to human health. Components like dietary fiber, polyphenols, and bioactive ingredients found in plant-derived foods play key roles. These substances help regulate blood sugar levels in diabetics by various mechanisms, including slowing carbohydrate digestion, stimulating insulin secretion, and enhancing glucose uptake in tissues (Matsinkou Soh et al., 2024).

Due to its physical properties and capacity to supply glucose, a crucial biomolecule commonly present in food, starch is essential for the growth of microorganisms in food products. These organisms can hydrolyse starch to release glucose, which serves as their primary fuel for development. Consequently, an increase in the amount of glucose can be an important and early indicator of contamination (Lopes et al., 2021).

Carbohydrates, fat, and protein are the three main energy sources; the former has the biggest effect on blood glucose levels. There is, however, no proof that there is a

© COPYRIGHT UPM

perfect balance between these three macronutrients for diabetics. The American Diabetes Association generally advises that an individual evaluation of one's present eating habits, preferences, and metabolic objectives should serve as the foundation for the macronutrient distribution (Kristensen et al., 2024).

The two primary factors affecting blood glucose in individuals with type 1 diabetes are exogenous insulin and diet. Carbohydrates have a greater impact on blood glucose levels compared to other energy sources in foods, such as fats and proteins. There is, however, no data indicating that there is a perfect balance between these three macronutrients for diabetics. The American Diabetes Association generally advises that the allocation of macronutrients be determined by an individual evaluation of existing dietary habits, preferences, and metabolic objectives (Elsayed et al., 2023).

Functional foods are natural or processed foods that comprise active components, which may or may not be fully understood. When eaten in safe, effective amounts, they offer proven health benefits, helping to thwart, manage, or treat lingering diseases (Martirosyan & Singh, 2015). Foods can be natural, like fruits, vegetables, nuts, legumes, and seafood, or processed, like fortified food products. They can come from plants, such as rice, soy, flaxseed, and garlic, or animals, like fish and dairy products. Some foods are also enhanced for added value (Kayode et al., 2023). Some guidelines help manage blood sugar, cholesterol, and blood pressure, and improve daily blood sugar control. Despite the importance of nutrition in diabetes care, there is limited research on what people with type 1 diabetes eat and how well they follow recommendations. More is known about insulin's effects and how it's delivered than about the eating habits of those with type 1 diabetes (Maahs & Clements, 2020). Eating

© COPYRIGHT UPM

carbohydrates that are released slowly into the blood can help manage diabetes and its complications by keeping blood sugar levels stable. Diets with these types of carbohydrates lower glucose and insulin levels throughout the day and might improve the body's ability to break down blood clots, which could help treat type 2 diabetes (T2D). When adding syrup to a diabetic diet, sucrose is a better choice than fructose. A study showed that replacing other carbs with fructose improved blood sugar control without affecting insulin, but a diet high in sucrose or fructose isn't recommended for people with diabetes or glucose issues. Additionally, foods high in fiber, certain proteins, or fats can affect how quickly carbs are digested and absorbed, which may benefit people with T2D (Guo et al., 2020).

2.5 Fluorescent-Based Non-Enzymatic Detection of Uric Acid and Glucose for Biomedical Application

Non-enzymatic detection of uric acid and glucose commonly employs fluorescent probes to selectively identify these metabolites based on their interactions with the probes. For uric acid detection, fluorescent materials, such as graphene oxide or organic dyes, serve as probes that exhibit fluorescence quenching when uric acid binds to them. This quenching can occur through various mechanisms, including physical adsorption onto the probe's surface or resonance energy transfer, which alters the probe's electronic structure and reduces emitted light intensity. The extent of this decrease in fluorescence is directly proportional to uric acid concentration, enabling precise quantitative analysis through calibration curves (Chen et al., 2024; Guan et al., 2014).

© COPYRIGHT UPM

Non-enzymatic detection of uric acid and glucose provides notable benefits compared to enzymatic methods, especially regarding stability, affordability, and ease of operation. Unlike enzymatic sensors that depend on biological enzymes such as uricase or glucose oxidase, which can deteriorate over time, non-enzymatic sensors employ inorganic materials, nanostructures, or chemical techniques that are naturally more robust and less affected by environmental conditions like temperature, pH, and humidity (Jarnda et al., 2023; Joshi & Slaughter, 2025). This improves their lifespan and ensures consistent performance. Moreover, producing non-enzymatic sensors bypasses the costly processes of enzyme purification and immobilization, making them more economical and suitable for large-scale commercial use. With direct analyte interaction, these sensors achieve a wider detection range and quicker response times, eliminating the intermediate stages seen in enzymatic methods. Additionally, non-enzymatic sensors can be engineered to endure challenging conditions, broadening their applicability to areas such as point-of-care diagnostics and industrial monitoring (Hassan et al., 2021; Cao et al., 2023).

In the case of glucose detection, fluorescent dyes like boronic acid derivatives are often used due to their ability to form reversible covalent bonds with glucose hydroxyl groups. The binding of glucose can lead to significant changes in the probe's fluorescence properties, either enhancing or quenching its emission. This phenomenon results from conformational changes within the fluorescent dye upon interaction with glucose. The fluorescence intensity or wavelength alterations provide reliable glucose level measurements when analysed using fluorometric techniques. Overall, non-enzymatic detection methods for uric acid and glucose leverage specific molecular interactions to achieve sensitive and selective quantification, making them valuable tools in biomedical diagnostics and monitoring (Du et al., 2019).

© COPYRIGHT UPM

2.6 Progress in the development of uric acid and glucose sensors

The determination of uric acid and glucose levels has evolved significantly over time. Early detection methods relied on the phosphotungstic technique (Ma et al., 2023). Over time, various analytical techniques such as optical, electrochemical, high-performance liquid chromatography (HPLC), gas chromatography, and capillary electrophoresis emerged, enabling more precise and diverse means of detection.

Electrochemical sensors have gained attention due to their high sensitivity and rapid response, making them well-suited for integration into wearable and flexible devices. These sensors offer real-time monitoring capabilities, providing valuable insights into metabolic activities (Liu et al., 2019; Ma et al., 2023). On the other hand, optical sensors have been widely adopted due to their simplicity, affordability, and resistance to external interferences. These include colorimetry, fluorescence, chemiluminescence, surface-enhanced Raman spectroscopy (SERS), and surface plasmon resonance (SPR), which have been extensively explored for uric acid and glucose analysis (Zhou et al., 2021). Detection instruments such as microplate readers, spectrophotometers, fluorescence spectrometers, Raman spectrometers, and surface plasmon resonance (SPR) instruments utilise optical signals, including colour changes, fluorescence variations, and spectral shifts, to achieve accurate measurements (Gerdan et al., 2022; Kumari et al., 2018; Saqib et al., 2018).

Among optical sensors, fluorescence-based sensing has emerged as a leading technology due to its exceptional sensitivity, specificity, and versatility (Kerian & State, 2023). Fluorescence sensors leverage fluorescent dyes, quantum dots, or

© COPYRIGHT UPM

nanoparticles to detect uric acid and glucose at extremely low concentrations, making them particularly useful for early diagnosis and real-time health monitoring. They are adaptable for non-invasive applications, such as wearable devices that analyse sweat or saliva (Cells et al., 2011). Advancements in functionalised quantum dots, including silicon quantum dots synthesised through hydrothermal methods, have further enhanced their efficiency and selectivity. With their compact, portable, and accurate diagnostic capabilities, fluorescence sensors continue to lead in the field of biochemical sensing (Zhang et al., 2023).

2.7 Synthesis of silicon quantum dots (SiQDs)

Silicon Quantum Dots (SiQDs) can be synthesised using various techniques, including chemical etching, laser ablation, thermal decomposition, plasma synthesis, and electrochemical methods. Chemical etching involves the use of strong acids or bases to dissolve bulk silicon into nanodots, while laser ablation employs high-energy lasers to break down silicon targets into nanoparticles (Morozova et al., 2022). Thermal decomposition and plasma synthesis generate silicon quantum dots by breaking silicon precursors at high temperatures, often requiring expensive equipment and complex procedures. Electrochemical methods, on the other hand, involve the anodisation of silicon wafers to form porous silicon, followed by ultrasonic treatment to extract quantum dots. While these techniques can produce high-quality silicon quantum dots, they often involve harsh chemicals, high energy consumption, or intricate processing steps (Askari et al., 2022) .

© COPYRIGHT UPM

Among these methods, the hydrothermal technique stands out due to its simplicity, eco-friendliness, and cost-effectiveness. This method utilises a high-temperature and high-pressure aqueous environment, enabling precise control over the size, crystallinity, and surface properties of silicon quantum dots. Unlike other approaches that require complex purification steps or hazardous reactants, hydrothermal synthesis predominantly uses water as a solvent, making it an environmentally sustainable option (Yoshimura & Byrappa, 2020). Additionally, the ability to functionalise silicon quantum dots directly during synthesis enhances their stability and application potential in bioimaging, optoelectronics, and sensing. Due to these advantages, the hydrothermal technique is increasingly recognised as a superior method for scalable and high-quality silicon quantum dots production (Yoshimura & Byrappa, 2020; Askari et al., 2022).

2.8 Quantum dots

Quantum dots (QDs), nanoscale semiconductor crystals, were initially defined by Ekimov and Onushenko in a glass matrix in 1981, and their first application in biological imaging was reported in 1998 (Zhang et al., 2023). Quantum dots have since expanded into various fields such as solar cells, light-emitting diodes, photodetectors, computing, biomedical imaging, and other applications. Quantum dots are nanoparticles or nanocrystals ranging in size from 2 to 12 nm, typically consisting of a few hundred to thousands of atoms. Their distinctive optoelectronic characteristics are strongly influenced by their size, which determines their exceptionally high surface-to-volume ratio. Silicon nanoparticles, derived from one of the most bountiful elements in the Earth's crust, have many uses in several fields, such as biology,

© COPYRIGHT UPM

chemistry, and medicine. Mainly noteworthy are photoluminescent (fluorescent) silicon nanoparticles known for their outstanding optical stability and biodegradability in physiological fields (Matea et al., 2017; Zhang et al., 2023).

Through the advancement of silicon nanotechnology, silicon quantum dots (SiQDs) are among the types of quantum dots widely used in sensing and biosensing applications. The indirect bandgap in silicon's bulk form causes poor photoluminescence. Still, the quantum confinement effect in silicon quantum dots allows for effective fluorescence emission with a large quantum yield, which is also crucial to note here (Upadhyay et al., 2022).

Being inert, less toxic, copious, and inexpensive qualities, silicon nanodots can be a favourable alternative to conventional quantum dots. The usage of silicon nanodots in chemical analysis (Kim et al., 2017), fluorescent bioimaging (Huang et al., 2016; Wu et al., 2018), and biomedicine has been common up to this point (Montalti et al., 2014; Xiong et al., 2015). However, according to (Yi et al., 2013), most synthetic silicon nanodots are hydrogen-terminated, making them simple targets for oxidation. Hydrophilic ligands must be added to make these H-Si-ended silicon nanodots water-soluble, which takes time and is cumbersome. Few studies have also concentrated on sensitively detecting biological substances using label-free silicon nanodots, including those undoped (Chen et al., 2018).

2.9 Silicon quantum dots

Quantum dots (QDs) are considerably larger than organic dyes but offer superior luminescent properties, making them suitable for a variety of applications. QDs are

© COPYRIGHT UPM

typically synthesised using elements from group II-VI (such as CdS, CdSe, CdTe, ZnS), group III-V (like InAs, InP), group I-III-VI (e.g., $AgInS_2$, $CuInS_2$), or group IV (including C, Si, Ge) (Xu et al., 2016). Quantum dots are considered alloyed quantum dots, core-shell quantum dots, and core-type quantum dots (Bera et al., 2010). Due to advancements in silicon nanotechnology, silicon quantum dots are extensively used in sensing and biosensing applications, standing out among the various types of quantum dots. It's worth noting that silicon in its bulk form exhibits poor photoluminescence because of its indirect bandgap. However, silicon quantum dots overcome this limitation through quantum confinement, enabling them to emit fluorescence efficiently with a high quantum yield. While silicon nanoparticles were initially developed in the 1950s, the discovery of fluorescent porous silicon did not occur until the 1990s, credited to Canhamin (Bera et al., 2010). Compared to porous silicon nanoparticles, silicon quantum dots provide several benefits for biological applications due to their distinct optoelectronic properties, biocompatibility, chemical stability, high photostability, bright fluorescence, and water dispersibility (Figure 2.3).

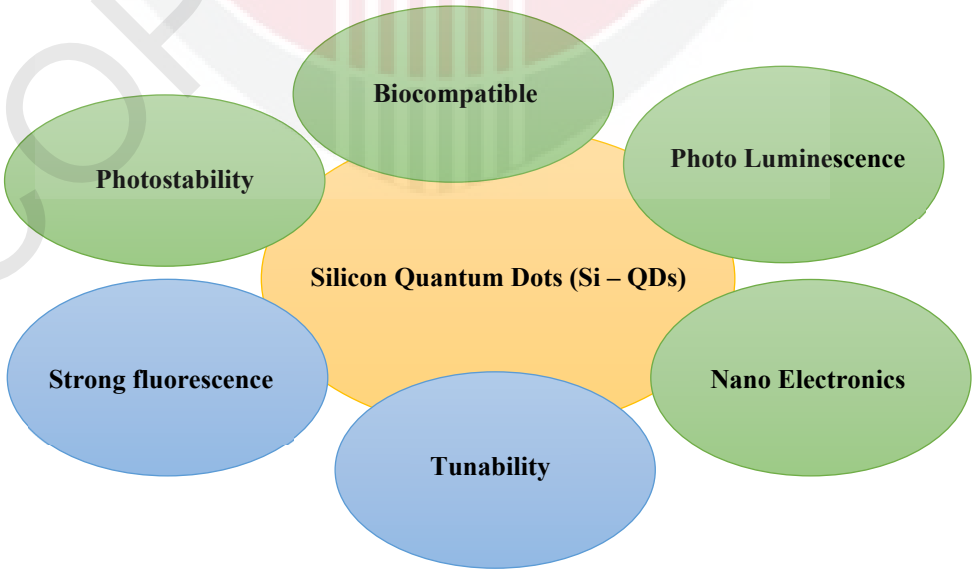

Figure 2.3: Importance of optoelectronic features of Si-QDs
(Upadhyay et al., 2022)

© COPYRIGHT UPM

As a result, there is growing research interest in silicon quantum dots for many types of applications, like, sensing and biosensing (Peng et al., 2018). Similar to other quantum dots, the fluorescence of the silicon quantum dot, exhibits a red shift as the size of the particle increases. Silicon quantum dots offer advantages over heavy metal-derived quantum dots obtained from group 2-6 elements, as they steer clear of toxicity concerns. Additionally, silicon quantum dots demonstrate excellent photoluminescence properties, especially when they are small in size (<10 nm). In trace amounts, silicon occurs in the human body as orthosilicic acid, which is biodegradable and easily eliminated via urine. Another reason for the increasing interest in silicon quantum dots is their ease of production and strong covalent bonding, making these nanocrystals stable and suitable for numerous applications under various conditions (Peng et al., 2018).

The behaviour of silicon particles is greatly influenced by their wide variety of dimensions, which range from a few nanometers (2 - 10 nm) to micrometers. They can also exist in non-porous or porous structures, as well as in amorphous or crystalline forms (Figure 2.2). The smaller silicon nanoparticles, which are usually less than 10 nm, are also known as silicon quantum dots (SiQDs), and their size-dependent bandgap and photoluminescent characteristics are well-established. Silicon quantum dots have been thoroughly investigated by researchers for a range of uses, such as sensors, bioimaging, light-emitting diodes (LEDs), and thermognostic applications.

Conversely, non-porous silicon nanoparticles (SiNPs) show unique optical and magnetic characteristics. Their diameters vary from 10 nanometers to many hundreds of nanometers. Being dielectric nanoparticles with a high refractive index of ~3.42 or

© COPYRIGHT UPM

lower, SiNPs offer a novel approach to controlling and enhancing light at the nanoscale (Mukrimaa et al., 2016).

Research worldwide has extensively investigated both silicon and silica nanoparticles for various uses, including diagnosing and treating diseases. Silicon nanoparticles can come in nonporous or porous forms, degrade quickly in water, and become luminescent when exposed to air. Mesoporous silica nanoparticles are the most studied type of silica nanoparticles, known for their large surface areas, adjustable porosity, and simple ways to modify them. Both types of nanoparticles break down in water into a form that can be easily eliminated through urine, which research suggests helps maintain bone health. Flavin adenine dinucleotide Drugs (FAD) have classified silica as "generally recognized as safe" for more than fifty years, and it is being used as a food additive in a wide range of products (Huang et al., 2022). The advantages of silicon and silica-based NPs over other materials are their high biocompatibility, inert degradation products, and adjustable hydrolytic degradability in relevant settings (from several hours to days or weeks).

Furthermore, researchers have engineered organic-inorganic siliceous nanoparticles with specific characteristics like well-defined pore structures and particular organic features for particular uses. This comparison involves two types: bridging silsesquioxane ($SiO_{1.5}$-R-$SiO_{1.5}$) nanoparticles and organically doped silica nanoparticles, both physically and chemically altered (Figure 2.4a, b). These nanoparticles, whether porous or nonporous, have been tailored with organic doping to break down under conditions relevant to biological systems, such as the presence of enzymes or bioreducing agents. Additionally, (Figure 2.4e), the study examines

© COPYRIGHT UPM

mesoporous silica nanoparticles doped with inorganic materials (Croissant et al., 2017).

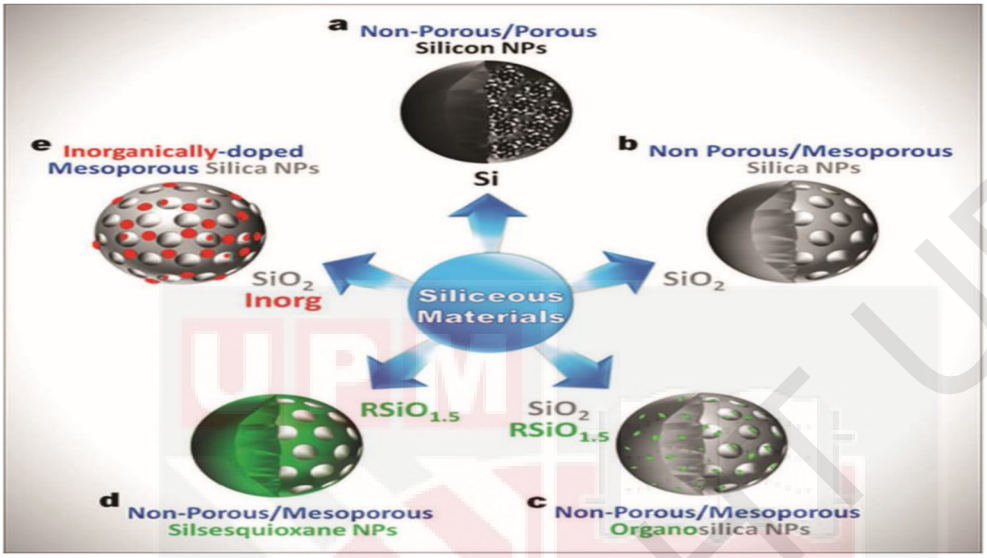

Figure 2.4: Shows different Si-containing NPs represented in a picture
(Croissant et al., 2017)

2.10 Sensors

Chemical sensors convert chemical data into an analysable signal that can be used to determine anything from the concentration of individual sample components to the general constituents of the sample. In chemical sensing, interactions between targets and sensing platforms lead to alterations in physical and chemical properties, which are then measured to identify the chemical constituents within a system. Different data acquisition methods, such as thermal, electrochemical, potentiometric, and optical techniques, have been employed to create various types of chemical sensors based on this specific interaction. Additionally, chemical sensors can be categorized according to the materials used in their sensing devices, including nanostructure-based sensors, carbon nanotube-based sensors, biological system-based sensors, and graphene-based

© COPYRIGHT UPM

sensors. Traditionally, chemical sensors are classified based on their mode of data transduction, which includes electrochemical signals, optical responses, electrical outputs, optical outputs, changes in electrical properties, and changes in mass (Kim et al., 2024).

Analyte, biorecognition element, and transducer comprise most of a biosensor. The biorecognition element facilitates the rapid and precise detection of analytes, and its interaction is reflected in physical and chemical characteristics which directly vary with differences in analyte concentration through the transducer. The Latin word "transducers," meaning to transmit or translate, is the root of the word "transducer." A transducer is a device that converts information from one type of system (for instance, chemical) to another (for instance, current). As shown in Figure 2.5, a recognition layer that consists of diverse biomaterials to synthetic biomimetic materials (similar in style to those of biological origin) has been developed and employed for sensitive and selective biosensors (Luka et al., 2015).

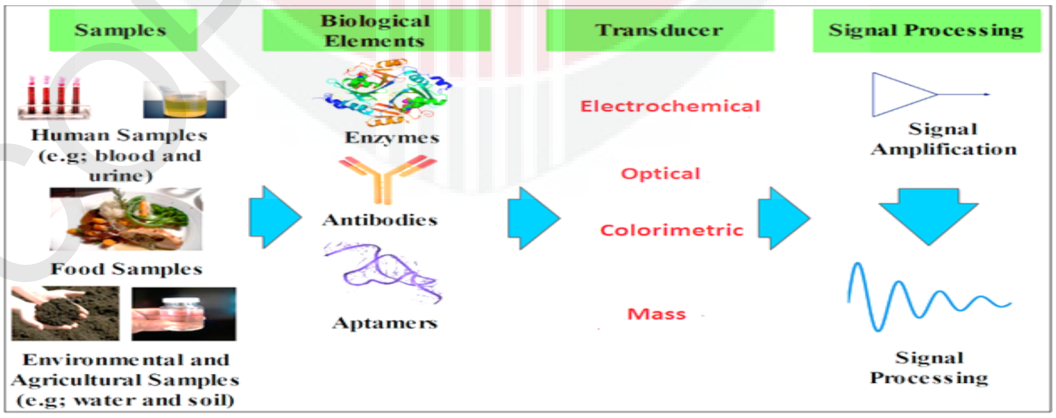

Figure 2.5: Schematic showing the many constituents of a biosensor, including the transducers, sensors, and biological identification elements
(Luka et al., 2015)

Based mainly on their mode of operation, glucose sensors can be categorized as either non-enzymatic, utilizing metals, metal oxides, or other substances that emulate enzymes, or enzymatic, involving enzymatic reactions. These sensors detect glucose indirectly by observing changes in properties such as fluorescence, band gaps in enzymes, or cyclic voltammetry, often through the formation of hydrogen peroxide (Teymourian et al., 2020). The mechanism of enzymatic and non–enzymatic sensors vary greatly, beyond just modification of the reactive element (whether it is an enzyme or enzyme–imitating material). In enzymatic glucose sensing, electrons are frequently transferred during oxidation events involving glucose nanomaterials and enzyme glucose oxidase (GOx). GOx contains the redox-active coenzyme flavin adenine dinucleotide (FAD), which catalyses the transformation of glucose into gluconolactone, which is characteristic of flavin enzymes. During the process, the enzyme converts GOx (FAD) into GOx ($FADH_2$), leading to changes in current that are then measured by the electrodes. Generally, GOx (FAD) + glucose → gluconolactone + GOx ($FADH_2$) is the reaction strategy (Figure 2.4), (Gao et al., 2021).

To grasp the operational mechanics of a standard non-enzymatic sensor (depicted in Figure 2.6) and the fundamental principle of glucose selectivity, an illustration featuring a metal oxide nanoparticle is included. This nanoparticle acts as an electrocatalyst, enabling electron transfer during the oxidation process of glucose. Metal oxide nanoparticles like Cu_2O, which interact with glucose, conduct electron transfer through a sequence of steps. Initially, copper (I) in Cu_2O undergoes electro-oxidation to form copper (II) species, which then progresses to copper (III) species in the presence of an alkaline solution. During these transformations, as glucose is oxidized to gluconic acid, copper (II) and copper (III) are reduced back to copper(I),

© COPYRIGHT UPM

with copper (III) acting as an electron transfer mediator. The specificity of these non-enzymatic sensors for glucose depends on the extent of the glucose oxidation reaction, initially observed in an acidic environment. The reaction of the metal oxide nanoparticle is outlined in the following scheme:

$$Cu_2O + 2OH^- + H_2O \rightarrow 2Cu(OH)_2 + 2e^- \quad (2.3)$$

$$Cu(OH)_2 \rightarrow CuO + H_2O \quad (2.4)$$

$$CuO + OH^- \rightarrow CuOOH + e^- \quad (2.5)$$

$$CuOOH = glucose \rightarrow Cu(OH)_2 + gluconic\ acid \quad (2.6)$$

In recent years, there has been increasing interest in non-enzymatic sensors compared to enzymatic ones. Enzymatic sensors often face challenges such as inconsistent performance due to pH and humidity variations, enzyme degradation leading to stability issues, and higher production costs. In contrast, non-enzymatic sensors offer greater stability and accuracy over longer periods. To overcome these issues, new technologies like photo-induced electron transfer, fluorescence resonance energy transfer (FRET), and optical sensors utilizing fluorescence have emerged. These advancements aim to develop highly accurate and sensitive glucose sensors for both minimally invasive and non-invasive detection methods (Aggas et al., 2020).

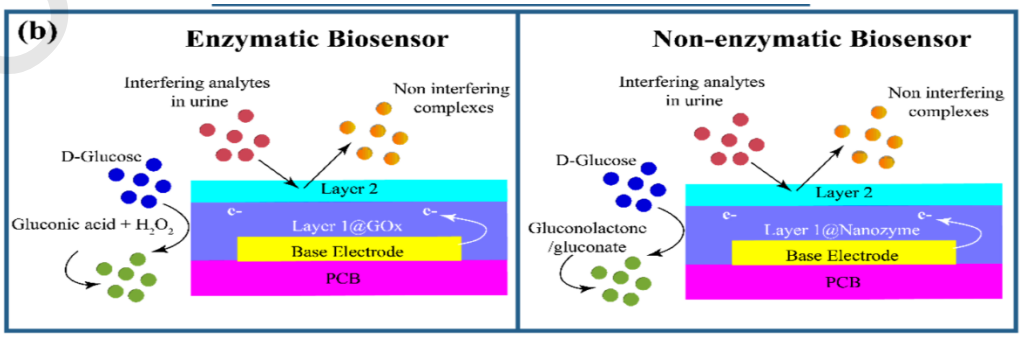

Figure 2.6: Diagram illustrating operational mechanisms in enzymatic and non-enzymatic biosensors
(Aggas et al., 2020)

© COPYRIGHT UPM

2.11 Silicon Quantum Dots as Fluorescent Biosensors: Applications in Bioimaging and Molecular Detection

To effectively use silicon quantum dots in biomedical applications, they require high visible photoluminescence efficiency and rapid radiative recombination rates. They must also be water-soluble and hydrophilic to prevent precipitation and aggregation in biological environments. The solubility depends on the surface termination method used, which changes their internal electronic structure and significantly affects emission wavelength and radiative lifetime. Silicon quantum dots passivated with oxide surfaces typically release yellow-red light due to dipole-forbidden transitions, with radiative lifetimes starting from 10^{-3} to 10^{-6} seconds. Their slow recombination rates limit their suitability for biological imaging. In contrast, silicon quantum dots passivated with hydrogen or carbon surfaces exhibit fast recombination rates (10^{-8} to 10^{-9} seconds) and feature direct band gap transitions that result in blue photoluminescence (Warner et al., 2005).

Zero-dimensional silicon quantum dots have garnered significant attention in sensing and bioimaging, often seen as alternatives to traditional organic dyes and semiconductor quantum dots. It is important to note that silane-based carbon dots have advantages over other fluorescent nanomaterials and similar photoluminescence properties, including low or nontoxicity, great photostability, notable biocompatibility, and earthiness. (Liu et al., 2022).

Because of these benefits, silicon quantum dots are frequently employed in bioimaging (Geng et al., 2018), biosensors(Gao et al., 2018), biomarkers, and fluorescence measurements of pH, Fe^{3+}, TNT, glyphosate, and other materials (Liu et al., 2022).

© COPYRIGHT UPM

Silicon quantum dots emitting in the blue to green spectrum have primarily been synthesized using the hydrothermal method. This process involved using various silicon sources, comprising 3-aminopropyl triethoxysilane (APTES), 3-aminopropyl trimethoxysilane (APTMS), 3-[2-(2-aminoethyl amino) ethylamino] propyl-trimethoxysilane (AEEA), N-[3-(trimethoxysilyl)propyl]-ethylenediamine (DAMO), N-trimethylsilyl imidazole, and diamino silane. These were combined with reducing agents such as trisodium citrate, catechol, ferulic acid, and ascorbic acid (AA). Additionally, alternative methods like microwave process, pulsed laser ablation, and electrochemical etching of Silicon have been used in Silicon quantum dots production. Label-free Silicon quantum dots have found direct applications in sensing, but they are also enhanced by post-decorating them with appropriate dyes, nanoparticles, or ligands. Yu et al. (2020) proposed a novel method to selectively detect the plant flavonoid rutin utilizing silicon quantum dots in the presence of BSA. The inclusion of BSA successfully inhibits the interaction of other evaluated flavonoids. However, the reaction between rutin and oxyhydroxide nanoparticles (CoOOH NPs) activates the Inner Filter Effect (IFE) mechanism and surface energy transfer with silicon quantum dots, leading to fluorescence quenching at λem = 450 nm (Lu et al., 2019).

Numerous straightforward techniques for detecting glucose have been developed using silicon quantum dots because it's essential to monitor glucose levels in the body to understand the progression and control of diabetes. Chen et al., (2018) utilized silicon quantum dots to develop a light-based sensor that detects changes in blood glucose levels. In their method, silicon quantum dots react with glucose oxidase, an enzyme that aids in converting glucose into gluconic acid and hydrogen peroxide. The fluorescence of silicon quantum dots is strongly influenced by hydrogen peroxide,

© COPYRIGHT UPM

which captures electrons from the quantum dots, resulting in reduced fluorescence. Furthermore, the acidity caused by gluconic acid also reduces the fluorescence of silicon quantum dots. This approach allows for glucose level measurements with an accuracy of about 0.54 mM. As depicted in Figure 2.5, glucose was detected down to 0.97 mM using a comparable method with amine-functionalized Silicon quantum dots. A slight modification involved measuring glucose using o-phenylenediamine (ODP) and glucose oxidase. In this process, ODP undergoes enzymatic conversion to 2,3-diaminophenazine (DAP) with the production of H_2O_2. The enzymatic activity generates hydrogen peroxide (H_2O_2), which in turn transforms o-phenylenediamine (ODP) into 2,3-diaminophenazine (DAP). The production of DAP reduces the fluorescence of silicon quantum dots (Si-QDs) through the inner filter effect (IFE) mechanism. A glucose-low limit of detection (LOD) of 0.35 mM is achieved through this technique. Monitoring hydrogen peroxide is important because of its biological importance. Zhu et al. (2020) developed a fluorescence quenching sensor for H_2O_2 using silicon quantum dots and silver nanoparticles (AgNPs). The energy transfer from silicon quantum dots to AgNPs resulted in fluorescence quenching at 450 nm. When exposed to H_2O_2, the dissolution of AgNPs reinstated the fluorescence of silicon quantum dots, allowing the measurement of H_2O_2 down to 1.5 mM. A novel approach for H_2O_2 sensing was introduced utilizing MnO_2 nanosheets as a nano-quencher (Li, Zhang, et al., 2020). The amino-terminated polyethylene glycol (PEG-NH_2) underwent modification onto MnO_2 nanosheets and was then combined with silicon quantum dots. The introduction of H_2O_2 reduced the (MnO_2-PEG-NH_2) to Mn^{2+} ions, subsequently restoring the fluorescence of silicon quantum dots with a sensitivity limit of 4.04 mM. A new technique has been devised to detect hydrogen peroxide, where the fluorescence of silicon quantum dots is initially suppressed by permanganate via

© COPYRIGHT UPM

the inner filter effect (IFE). Subsequently, fluorescence is restored through the redox reaction between permanganate and hydrogen peroxide (Upadhyay et al., 2022).

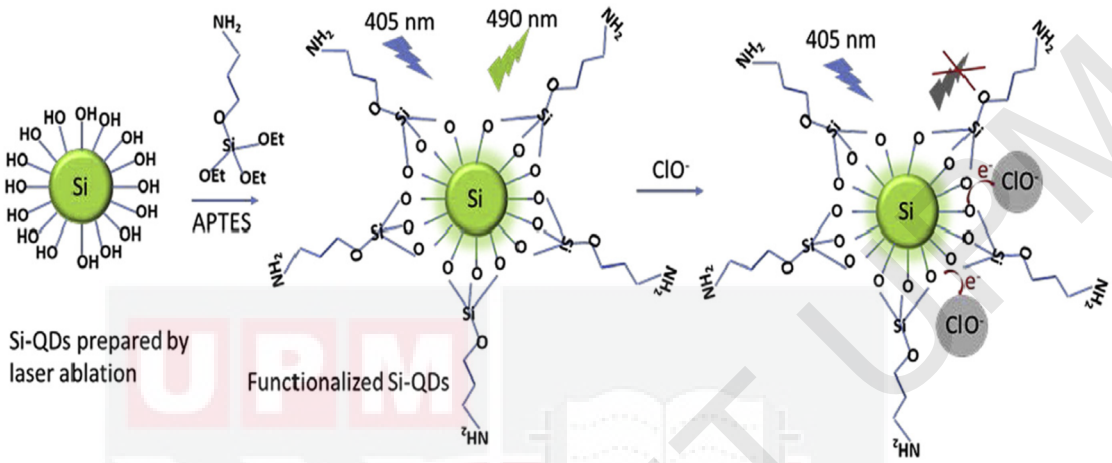

Figure 2.7: Preparation of functionalized Si-QDs for the detection of ClO^- (Upadhyay et al., 2022)

Metal cation detection via fluorescence relies on fluorescence quenching caused by interactions with carbon dots. This interaction can be classified into static and dynamic quenching. Static quenching involves the formation of a non-emissive complex between the carbon dot and the metal cation, resulting in the previously emitting state returning to the ground state without emitting photons. An increase in the quencher concentration usually changes the absorbance spectra without affecting fluorescence lifetimes, suggesting a static quenching mechanism. Additionally, higher system temperatures generally decrease quenching. When a metal cation interacts with an excited-state carbon dot, energy transfer occurs, causing the carbon dot to return to its ground state without emitting photons. This phenomenon is referred to as dynamic quenching, also known as collisional quenching. In dynamic quenching, an increase in quencher concentration typically alters fluorescence lifetimes but not absorbance spectra. Additionally, higher system temperatures generally increase quenching

effects. Various mechanisms contribute to dynamic quenching, such as surface energy transfer (SET), Förster resonance energy transfer (FRET), and photo-induced electron transfer (PET). The inner filter effect (IFE) is another quenching mechanism mentioned, which is non-molecular and dependent on the concentration (Noun et al., 2021).

Water-soluble silicon quantum dots have been successfully synthesized, leading to the development of a diverse range of photoluminescent biosensors (Zhang et al., 2023). These biosensors have been specifically designed to detect target analytes such as lactate dehydrogenase, hydrogen ions, glucose, heavy metal ions, DNA, thiols, and microorganisms. The sensing mechanisms of silicon quantum dots-based biosensors utilize a range of techniques, such as surface energy transfer (SET), fluorescence resonance energy transfer (FRET), metal-enhanced fluorescence (MEF), the inner filter effect (IFE), and others. Various design approaches have been employed in developing these biosensors (Zhang et al., 2023). Here, the summary of methods focuses on how different substances impact the brightness of light emitted by silicon quantum dots, as well as combining them with other materials or molecules and using biological methods to alter them. Table 2.1 provides a summary of the activities of Silicon quantum dots-based biosensors in detecting different analytes (Zhang et al., 2023):

© COPYRIGHT UPM

Table 2.1: Overview of silicon quantum dots–based sensor performance

Sample type	Target molecule	Excitation (nm)/Emission (nm)	Sensitivity (LOD)(nM)	Dynamic range	Reference
Tap water	$Cr_2O_7^{2-}$	362 /437	180	0.5 – 100 μM	Wen et al., 2021
Aqueous	Hg^{2+}	347 /440	24	0.1 – 4 μM	Shen et al., 2019
Live Cells	pH	365 /440	NA	pH 5 – pH 10	Na et al., 2021
Aqueous	DNA	359 /601	4.3	20 – 1500 nM	Na et al., 2021
MCF-7 cells	MUC1	359 /670	1.52	3.33 – 250 nM	Zhang et al., 2018

Noted: NA – not applicable

© COPYRIGHT UPM

Numerous works highlight the advantages of silicon quantum dots in detection, emphasizing their fast, simplicity, and great selectivity. These works also implement a potential route for improving food management and safety. A fluorescence method was developed to detect rutin in traditional Chinese herbs using water-dispersed silicon nanoparticles (SiNPs) and bovine serum albumin (BSA). Ferulic acid serves as the reducing agent in this technique. Both rutin and quercetin can effectively quench the fluorescence of silicon nanoparticles. The fluorescence response decreases as rutin concentration increases, with a detection limit of 0.04 μM and a concentration range of 0.33–33.30 μM. The quenching mechanism of rutin for silicon nanoparticles has been studied and is primarily attributed to the inner filter effect fluorescence method that was developed to detect rutin in traditional Chinese herbs using water-dispersed silicon nanoparticles and bovine serum albumin (BSA). Ferulic acid serves as the reducing agent in this technique. Both rutin and quercetin can effectively quench the fluorescence of SiNPs. The fluorescence response decreases as rutin concentration increases, with a detection limit of 0.04 μM and a range of 0.33–33.30 μM. The quenching mechanism of rutin for Silicon nanoparticles has been studied and is primarily attributed to the inner filter effect (Yu et al., 2020).

Lu et al., (2019), reported that blue fluorescence in silicon nanoparticles (SiNPs) is quenched by CoOOH nanoparticles (NPs) owing to a redox interaction between the vitamin C diol group and CoOOH NPs, leading to the breakdown of the NPs. They developed a fluorometric technique for precise vitamin C detection, which offers a low detection limit of 0.47 μM and a linear response in the concentration range of 0.5 μM to 20 μM.

© COPYRIGHT UPM

According to Liu et al., (2021a), a straightforward one-pot procedure was used to successfully synthesize cyan fluorescent silicon quantum dots to detect chlorogenic acid (CGA) quickly. Because of the combined dynamic and static quenching mechanisms, the overall emission intensity of the Silicon quantum dots was effectively quenched when chlorogenic acid was applied. Notably, the limit of detection (LOD) was 0.43 µmol/L, and the fluorescence quenching efficiency showed a linear correlation across a broad concentration range of 10 to 150 µmol/L. Additionally, the proposed silicon quantum dots were effectively utilized to measure chlorogenic acid in coffee beans and instant coffee, yielding satisfactory results after a simple pre-treatment process.

A novel ratiometric fluorescence sensing device was developed to detect Hg^{2+} with extremely high sensitivity using rhodamine B and amino-functionalized silicon nanoparticles, which produce two distinct fluorescence emission peaks at a single excitation wavelength. Rhodamine B's fluorescence remained unaffected by Hg^{2+}, while the fluorescence of the amino-functionalized silicon nanoparticles was selectively quenched by Hg^{2+}. A detection limit of 3.3 nM was attained, and the ratio of fluorescence intensities linearly declined with rising Hg^{2+} concentrations from 0.005-0.1 µM and 0.1-7 µM within 0.5 min. The ratiometric fluorescence sensing system demonstrated strong selectivity for Hg^{2+} in complex water samples, with minimal interference and vital application (Wu et al., 2018).

Also reported is a water-soluble and P^{H}-responsive silicon nanodot that was hydrothermally synthesized for fluorometric glucose detection. Silicon nanodots as glucose sensors offer hydrogen peroxide-quenching and gluconic acid-sensitive

© COPYRIGHT UPM

fluorescence, enhancing glucose detection and sensing. The method allowed for glucose measurement in serum samples with high selectivity, detecting glucose concentrations as low as 0.54 μM (Chen et al., 2018).

A ratiometric DNA sensor was synthesized using fluorescent silicon nanodots (SiNDs), and $Ru(bpy)_2(dppx)^{2+}$ (Zhang et al., 2021). The sensor exhibits significant overlap between SiNDs' excitation and emission spectra and $Ru(bpy)_2(dppx)^{2+}$ absorption spectrum, allowing fluorescence quenching towards SiNDs. The method is sensitive, fast, and accurate, with a linear fluorescence intensity ratio in aqueous solutions, and the method's precision and limit of detection are 3.5% (50 nM, n = 13) and 4.3 nM, respectively. The sensor can visually identify trace DNA, with recoveries ranging from 98% to 119%.

Fluorescent silicon nanoparticles (SiNPs) were developed using 4-aminophenol and N-aminoethyl-aminopropyltrimethyl as reducing agents and silicon sources through a one-pot hydrothermal method. These SiNPs serve as pH-sensitive probes to study changes in living cells. The fluorescence intensity increased with the pH of the solutions, with a response range from 5.0 to 10.0. The SiNPs are highly biocompatible and effectively visualize diseases linked to changes in intracellular pH (Na et al., 2021).

Utilizing differences in the fluorescence intensity of silicon quantum dots (SiQDs), lactate dehydrogenase (LDH) activity was detected, as reported by (Zhou et al., 2022). Silicon quantum dots were synthesized using 3-aminopropyltrimethoxysilane (APTMS) as a source of silicon. In this system, the fluorescence of the silicon quantum

© COPYRIGHT UPM

dots was initially quenched by nicotinamide adenine dinucleotide (NADH), which was then restored by lactate dehydrogenase through its catalytic reaction that consumes NADH. A linear calibration curve for LDH was established within the range of 0.77–385 U/mL. The technique effectively measured lactate dehydrogenase levels in human serum samples and demonstrated excellent selectivity for lactate dehydrogenase detection.

A straightforward technique for examining oxytetracycline (OTC) in milk samples employs a luminescent sensor of silicon quantum dots (SiQDs). This sensor utilizes a single-step hydrothermal technique to measure OTC by leveraging the inner filter effect. The absorption characteristics of OTC overlap with the excitation spectrum of silicon quantum dots, resulting in decreased fluorescence intensity with higher OTC concentrations. The proposed method for detecting OTC in milk samples showed high recovery rates (ranging from 98.8% to 100.5%) and percentage low values of relative standard deviation (ranging from 0.93% to 2.31%) (Eda et al., 2020).

In a separate study, researchers employed F-doped silicon quantum dots to detect new coccine in food samples, utilizing a one-step hydrothermal method. By employing the Inner Filter Effect (IFE) principle, they quickly quenched the fluorescence intensity, reducing the process to just 1 minute. The F-SiQDs effectively identified new contaminants and produced accurate detection results after coating filter paper. Within the ranges of 1-100 µmol/L and 100-200 µmol/L, they measured the concentration of new coccine, with corresponding detection limits of 0.33 µmol/L and 0.18 µmol/L (Liu et al., 2022).

© COPYRIGHT UPM

Documented also is the hydrothermal synthesis of water-soluble fluorescent silicon quantum dots (SiQDs) using urea propyl triethoxysilane (UPTES) as the silicon source and sodium citrate as the deoxidizer. The silicon quantum dots made in this way had good emission and persistent fluorescence over a broad pH range of 2 to 14. These silicon quantum dots demonstrate remarkable resilience to changes in pH, salt concentration, and certain organic reagents, making them well-suited for biochemical detections. Specifically, they have proven highly sensitive in detecting formaldehyde, as formaldehyde effectively quenches the fluorescence of the silicon quantum dots via electron transfer between the carbonyl group of formaldehyde and the amino group on the surface of the QDs. This detection technique is simple, sensitive, and very impervious to influence from other materials (Xu et al., 2016).

An approach was employed to synthesize amino-functionalized silicon quantum dots (NH_2@SiQDs) utilising silicon tetrachloride and allylamine. These dots showed fluorescence yield, optical stability, and solubility in water. A non-enzymatic glucose biosensor was developed, with a linear relationship with blood glucose concentration and a detection limit of 3.0×10^{-7} mol/L (Du et al., 2019).

Developing an optical sensor using silicon quantum dots has become crucial for detecting uric acid and glucose in urine without relying on enzymes. This alternative method prioritizes increased sensitivity and selectivity, simplifying the process compared to enzymatic techniques. The silicon quantum dots, known for their biocompatibility, support miniaturization and integration for real-time, continuous monitoring. The cost-effectiveness and environmental friendliness of silicon make it a viable option, offering potential applications in diagnostics, personalized medicine, and health monitoring.

© COPYRIGHT UPM

Developing silicon quantum dots (SiQDs) for sensors, like detecting uric acid in urine and glucose in food, faces several challenges. These include making silicon quantum dots consistently, improving their surface to ensure selective and sensitive detection, and achieving high sensitivity in complex samples. Other key issues are providing stability, avoiding interference from other substances, enabling real-time detection, and addressing regulatory and commercialization requirements.

© COPYRIGHT UPM

CHAPTER 3

METHODOLOGY

3.1 Reagents

Table 3.1: List of reagents used in the experiment

Reagent	Source	Purity	Country
3-Aminopropyl triethoxysilane (APTES)	Aldrich	99.9%	USA
Ethylenediamine (EDA)	Aldrich	90%	USA
Trisodium citrate	Sigma	99%	USA
Nitrogen gas		99.9%	USA
Disodium phosphate	HmbG	98%	USA
Sodium hydroxide	Scharlau	50%	USA
Hydrochloric acid	Fisher	37%	USA
Uric acid	Sigma	99%	USA
Glucose	Sigma	99.5%	USA
Sodium hydrogen phosphate	Scharlau	99%	USA

3.2 Preparation of silicon quantum dots (SiQDs) via a one-pot hydrothermal technique

Water-soluble fluorescent silicon quantum dots were synthesised using a hydrothermal method based on the procedures of Eda et al. (2020), and Chan et al. (2018), with a modification incorporating a capping agent. In this synthesis, 1.104 g of sodium citrate was dissolved in 25 ml of deionised water that had been saturated with nitrogen gas to remove oxygen. Then, 6 ml of APTES was added as the silicon precursor, and 200 µl of ethylenediamine (EDA) was introduced as a capping agent to enhance stability and control particle size. The mixture was covered with aluminium foil and stirred thoroughly for 10 minutes using a magnetic stirrer.

© COPYRIGHT UPM

The resulting solution was transferred to a stainless-steel autoclave and heated at 180 °C for 5 hours. After cooling to room temperature, the transparent solution was dialysed against ultrapure water for 48 hours to remove impurities such as residual APTES and sodium citrate. The dialysed colourless liquid was then dried in an oven at 40 °C. Finally, the obtained yellow silicon quantum dots crystal was stored at 4 °C for future use. The product appeared yellowish in its solid form and colourless when dissolved in deionised water, exhibiting bright blue photoluminescence (PL) under UV light.

3.3 Characterisation of the prepared SiQDs

Characterisation of silicon quantum dots with UV/Vis, fluorescence, FTIR, HRTEM, and XRD techniques provides a comprehensive understanding of their electrical, optical, vibrational, morphological, and structural properties. This detailed knowledge is essential for designing and optimising the performance of quantum materials for applications in sensing.

3.3.1 UV/Vis Spectroscopy of SiQDs

To determine the UV-Vis absorption spectra of silicon quantum dots (SiQDs). First, 200 µl of a 0.5 mg/ml silicon quantum dots solution was pipetted into the first well of a white 96-well plate. In the second well, 150 µl of the 0.5 mg/ml silicon quantum dots solution was mixed with 50 µl of deionized (DI) water. In the third well, 100 µl of the 0.5 mg/ml silicon quantum dots solution was combined with 100 µl of DI water. A Thermo Scientific™ Multiskan™ GO microplate spectrophotometer was used to

© COPYRIGHT UPM

measure the UV-Vis absorption spectra of these samples within the wavelength range of 200 – 800 nm at room temperature. The spectra were recorded and the data to assess the optical properties of the silicon quantum dots was analysed.

3.3.2 Fluorescent Spectroscopy of SiQDs

The fluorescence spectra of silicon quantum dots (SiQDs) were acquired using a Tecan microplate reader equipped with Tecan black 96-well plates and SPARKCONTROL Magellan software. For the measurements, 250 µl of a 0.5 mg/ml silicon quantum dots solution was pipetted into the first well and mixed with 50 µl of 0.1 M phosphate buffer solution (pH 7.2). In the second well, 200 µl of the 0.5 mg/ml silicon quantum dots solution was mixed with 100 µl of the same buffer. Finally, the third well contained 50 µl of the silicon quantum dots solution and 250 µl of the buffer. All solutions were prepared, and measurements were taken at room temperature. Fluorescence measurements were recorded with an excitation wavelength of 305 nm and an emission wavelength of 350 nm, respectively.

3.3.3 Fourier-transform infrared spectroscopy (FTIR)

Fourier-transmission infrared spectroscopy (FTIR) is crucial for analysing surface chemistry, determining functional groups, and the interaction between the components in the sample. This knowledge is essential for tailoring these nanomaterials for applications in optoelectronics, bioimaging, and other emerging fields.

© COPYRIGHT UPM

The surface functional groups of the synthesized silicon quantum dots were determined using Fourier Transform Infrared Spectroscopy (FTIR) with the Bruker ATR-FTIR Alpha spectrometer (Germany). Initially, 5 mg of the silicon quantum dots were weighed and thoroughly mixed with approximately 100 mg of potassium bromide (KBr), a spectroscopically pure, infrared-transparent material. The mixture was finely ground in an agate mortar and pestle to ensure homogeneity and prevent scattering artifacts. Once a uniform powder was achieved, it was transferred to a pellet press, where sufficient pressure (typically 5-10 tons) was applied to form a transparent pellet. The pellet was then carefully placed in the sample holder and aligned properly. The FTIR spectrum was recorded across the relevant wavenumber range (4000–400 cm^{-1}) to identify characteristic absorption peaks corresponding to functional groups, such as hydroxyl (-OH), carbonyl (C=O), or siloxane (-Si-O-Si) on the silicon quantum dots surface. The resulting spectrum was analysed by comparing the observed peaks with standard functional group reference data (Kumar et al., 2019).

3.3.4 High-Resolution Transmission Electron Microscope (HRTEM)

For morphological and size analysis, a small quantity (2 mg) of silicon quantum dot crystals was dispersed in ethanol, used as a suitable solvent, and briefly sonicated to ensure a uniform suspension. A drop of the suspension was deposited onto a carbon-coated copper grid and allowed to dry under ambient laboratory conditions (room temperature and atmospheric pressure) or in a vacuum. The grid was then analysed using the JEOL JEM2100F Field Emission TEM (Japan), operated at a high voltage (200 kV), to capture high-resolution images that revealed the quantum dots' size, shape, and lattice fringes. Particle size distribution was measured from the images

© COPYRIGHT UPM

using the software ImageJ, providing detailed insights into the size uniformity and crystallinity of the quantum dots (Igathinathane et al., 2008; Zhang & Wang, 2023).

3.3.5 X-ray diffraction (XRD)

The target sample is ground to a finer particle size for the structural analysis of silicon quantum dots and placed in the XRD sample tray. The analysis was carried out using the Shimadzu XRD6000 (Japan) equipped with Cu-Kα radiation with a maximum voltage of 60 kV and a maximum current of 60 mA. A scan was performed over the 2θ range of 10°–80° to identify crystalline phases and lattice structures. The resulting diffraction pattern was analysed to determine the peak positions corresponding to the crystallographic planes of silicon. Scherrer's equation was applied to calculate the crystallite size using the dominant peaks' full width at half maximum (FWHM), confirming crystallinity and particle dimensions (Du et al., 2019).

3.4 Phosphate buffer preparation

A working buffer solution of 0.1 M was prepared by following these steps: 3 g of NaH_2PO_4 was measured and dissolved in 250 ml of deionized water (monobasic), and 3.55 g of Na_2HPO_4 was measured and dissolved in 250 ml of deionized water (dibasic). These two solutions were then employed to produce various pH solutions for the experiment. The procedure for preparing the buffer solutions is detailed in Table 3.2.

© COPYRIGHT UPM

Table 3.2: Preparation of working buffer solutions

pH	Na_2HPO_4 (dibasic) ml	NaH_2PO_4 (monobasic) ml
7.0	30.50	19.50
7.4	40.50	9.50
8.0	47.35	2.65
8.5	45.59	4.41
9.0	37.03	12.97
9.5	21.69	28.31
10.0	0.45	49.55

Dibasic and monobasic solutions (Table 3.2) were mixed and diluted to a final volume of 100 by adding deionized water. The pH of each buffer solution was then adjusted to the desired values using a digital pH meter and 0.1 M NaOH and 0.1 M HCl solutions. Starting from the pH 7 buffer, buffers of pH 7.2, 7.4, 8.0, 8.5, 9.0, 9.5, and 10.0 were created by incrementally adding NaOH solution until the target pH was reached using a digital pH meter.

3.5 Preparation of uric acid and glucose solutions

Various concentrations of freshly prepared uric acid solutions were used throughout the experiment. Each concentration of the uric acid solutions (0.8, 0.6, 0.4, 0.2, 0.1, 0.05, 0.025, 0.0125, and 0.00625 mg/ml) was diluted in phosphate buffer. Exactly 8 mg of uric acid powder was carefully weighed and dissolved in 5 ml of phosphate buffer solution at pH 7.2. The mixture was heated to 60°C with stirring using a magnetic stirrer until the uric acid powder completely dissolved. The solution was then diluted with an additional buffer solution to bring the total volume to 10 ml, resulting in a uric acid solution with a concentration of 0.8 mg/ml. Subsequent solutions were prepared by diluting this stock solution of 0.8 mg/ml of uric acid.

© COPYRIGHT UPM

For the preparation of glucose solution (1 mg/ml), 10 mg of glucose powder using a precise weighing scale was measured and added to it was 10 ml of deionised water into a clean and dry container. The mixture was gently stirred until the glucose powder was completely dissolved. To prepare glucose solutions with various concentrations (0.8, 0.6, 0.4, 0.2, 0.1, 0.08, 0.06, 0.04, 0.02, and 0.01 mg/mL), the dilution formula $M_1V_1 = M_2V_2$ was used.

3.6 Optimisation Parameter

3.6.1 Determination of silicon quantum dots concentration

To determine a suitable concentration of the prepared silicon quantum dots for the analysis, a series of concentrations (2 mg/ml, 1.5 mg/ml, 1 mg/ml, and 0.5 mg/ml) of silicon quantum dots were analysed.

3.6.2 Effect of pH Buffer

A solution containing 0.5 mg/ml of silicon quantum dots was prepared to optimize various parameters. Initially, 10 mg of the dried silicon quantum dots powder was precisely weighed using an analytical balance. This powder was then diluted in 20 ml of phosphate buffer at the desired pH and subsequently sonicated for 15 minutes to achieve proper dilution and a uniform mixture. The resulting solution was shielded with aluminium foil and kept at 4^{o}C for upcoming use. All measurement was conducted in triplicate (n = 3).

© COPYRIGHT UPM

To optimise the pH of the phosphate buffer solution suitable for uric acid detection, various pH-adjusted phosphate buffer solutions were used. Using Tecan black 96-well plates, 200 µl of 0.1 M buffer (pH 7.0, 7.2, 7.4, 8.0, and 10) and 50 µl of 0.5 mg/ml SiQDs were used. A 50 µl freshly prepared uric acid solution (0.6 mg/ml) was added. The fluorescence emission was measured using a microplate reader after a 5-minute incubation at room temperature, with excitation and emission wavelengths set at 305 nm and 440 nm, respectively. All measurement was conducted in triplicate (n = 3).

To optimize the pH of phosphate buffer solutions suitable for detecting glucose, various pH-adjusted phosphate buffers (pH 7.0, 7.2, 7.4, 8.0, and 8.5) were used. Into a cleaned Tecan black 96-well plate, 250 µl of buffer was mixed with 50 µl of 0.5 mg/ml silicon quantum dots then into 3 different wells 200 µl of buffer solution was added 50 µl of 0.5 mg/ml silicon quantum dots and subsequent addition of 1 mg/ml glucose. Fluorescence emission was measured using a microplate reader after a 15-minute incubation time at room temperature, with excitation and emission wavelengths set at 305 nm and 440 nm, respectively. All measurement was conducted in triplicate (n = 3).

3.6.3 Effect of reaction time

To determine the maximum reaction time between 0.5 mg/ml silicon quantum dots and uric acid, a freshly prepared solution of 0.6 mg/ml of uric acid was made using a 0.1 M phosphate buffer solution of pH 7.2. The same procedure as described above was followed, but in this case, fluorescence intensity was recorded at time intervals of 0, 5, 10, 15, 20, 25, and 30 minutes. Fluorescence emission measurements were taken

© COPYRIGHT UPM

using a microplate reader with excitation at 305 nm and emission at 440 nm. All measurement was conducted in triplicate (n = 3).

To determine the optimal reaction time between 0.5 mg/ml silicon quantum dots and glucose, a freshly prepared glucose solution of 1 mg/ml was prepared using 0.1 M phosphate buffer solution of pH 7.2. The same procedure as described previously was followed, but in this instance, fluorescence intensity was measured at time intervals of 0, 5, 10, 15, 20, 25, 30, 35, and 40 minutes. Fluorescence emissions were recorded using a microplate reader with excitation at 305 nm and emission at 440 nm. All measurement was conducted in triplicate (n = 3).

3.7 Linearity study

A set of uric acid concentrations from 0.004 to 0.1 mg/ml was prepared to assess the response of the newly developed biosensor. In a Tecan black 96-well plate, 250 µL of phosphate buffer solution at pH 7.2 and 50 µl of a 0.5 mg/ml silicon quantum dots solution were combined as a control. For the test samples, 200 µl of phosphate buffer solution, 50 µl of a known concentration of uric acid, and 50 µl of the 0.5 mg/ml silicon quantum dots were pipetted and mixed (repeated in three different wells). After a 5-minute reaction period at room temperature, fluorescence intensity was measured. The fluorescence was monitored using excitation and emission wavelengths of 305 and 350 nm, respectively. A graph plotting fluorescence intensity against uric acid concentration was generated to assess the linearity of the calibration curve for the developed biosensor using fluorescence spectra measurement at 440 nm.

© COPYRIGHT UPM

To evaluate the response of the newly developed biosensor, glucose concentrations ranging from 0.01 to 1 mg/ml were prepared. In a Tecan black 96-well plate, 250 µL of phosphate buffer solution at pH 7.2 was mixed with 50 µL of a 0.5 mg/ml silicon quantum dots solution as a control. Additionally, 200 µL of phosphate buffer solution, 50 µL of a known glucose concentration, and 50 µL of the 0.5 mg/ml silicon quantum dots solution were pipetted and combined in five wells of Tecan black 96-well plate. After a 15-minute incubation at room temperature, the fluorescence intensity was measured. Fluorescence monitoring was performed at excitation and emission wavelengths of 305 nm and 440 nm, respectively. A graph was created to illustrate the relationship between fluorescence intensity and glucose concentration, determining the linearity of the calibration curve for the new biosensor using fluorescence spectra measurement at 440 nm.

3.8 Real sample analysis

A urine sample was gathered and spun at 10,000 rpm in a centrifuge for 10 minutes to eliminate impurities. The supernatant was poured away, and the deposit was then mixed with a phosphate buffer of pH 7.2 with a ratio of 1:9 (v/v) (1 ml of urine sample to 9 ml of buffer solution). After dilution, the sample was injected with different concentrations of uric acid solution (0.05 and 0.07 mg/ml). Fluorescence emission readings were conducted using a microplate reader, with an excitation wavelength of 305 nm and an emission wavelength of 440 nm. The measurement was performed in triplicate (n = 3).

© COPYRIGHT UPM

For glucose determination in juice products, a store-bought mango juice packet was processed by centrifuging at 10,000 rpm for 10 minutes. The deposit was then diluted 100 times by mixing 0.1 ml of juice with 9.9 ml of deionised (DI) water. Next, glucose solutions of 0.4 mg/ml and 0.6 mg/ml were added to the sample. Fluorescence emission readings were captured using a microplate reader, with excitation at 305 nm and emission at 440 nm. The measurements were conducted in triplicate (n = 3).

3.9 Interference study

Several species of ions (0.1 mg/ml of urea, ascorbic acid, creatine, glucose, potassium chloride, and sodium chloride) that may be found in the human urine system were selected for interference investigation. Foreign ions and uric acid (0.2 mg/ml) were introduced into the biosensor probe. The response to uric acid detection was measured in the presence of these foreign substances, and changes in fluorescence intensity were calculated to evaluate the effect of the foreign substrate on the biosensor's performance.

Various ions and compounds commonly present in the human body, including urea, ascorbic acid, creatinine, sodium chloride, and potassium chloride were selected to investigate their potential interference. All the selected ions and compounds were fixed at 0.1 mm/ml. These ions and compounds combined with glucose at 0.2 mg/ml were injected into the well consisting of 0.5 mg/ml silicon quantum dots in phosphate buffer pH 7. The sensor's ability to detect glucose was tested in the presence of each foreign substance, and the changes in fluorescence intensity were studied to determine their impact on the sensor's performance.

© COPYRIGHT UPM

3.9.1 Reproducibility study

To test the reproducibility of the sensor, the prepared silicon quantum dots were analysed using five different assays (n = 5). The silicon quantum dots were exposed to 0.2 mg/ml of uric acid and the fluorescence intensity of silicon quantum dots was recorded. The average, standard deviation (SD), and relative standard deviation (RSD) were calculated. A similar procedure was used for the determination of glucose**.**

© COPYRIGHT UPM

CHAPTER 4

RESULTS AND DISCUSSION

4.1 Synthesis of silicon quantum dots (SiQDs)

The synthesis of water-soluble fluorescent silicon quantum dots (SiQDs) in this study introduces a key modification by incorporating ethylenediamine (EDA) as a capping agent. This novel approach enhances the stability of the silicon quantum dots, prevents agglomeration, and allows for better control of particle size, ultimately improving their fluorescence properties. Compared to previous methods by Eda et al. (2020) and Chan et al. (2018), which lacked this specific stabilising agent, the modified synthesis results in silicon quantum dots with superior photoluminescence and water solubility. The synthesised silicon quantum dots exhibit a distinct yellow colour in solid form and appear colourless in solution, displaying bright blue fluorescence under UV light. This improvement not only refines the synthesis process but also broadens the potential applications of silicon quantum dots in bioimaging, sensing, and optoelectronics, making it a significant contribution to nanotechnology.

This study presents a one-step, eco-friendly, and cost-effective method for producing silicon quantum dots, using 3-aminopropyltriethoxysilane (APTES) as the silicon source and trisodium citrate as the reducing agent. Unlike previous studies that used bulk silicon or SiO_2, requiring additional functionalisation for water solubility, APTES provides a direct, water-soluble precursor that enhances photostability. The addition of EDA plays a crucial role in stabilising, passivating, and functionalising silicon

© COPYRIGHT UPM

quantum dots, directly influencing their size, optical properties, and compatibility with various applications. During high-temperature heating, trisodium citrate reduces siloxane molecules, leading to the formation of silicon crystal nuclei (Zhou et al., 2022, Eda et al., 2020). Figure 4.1 illustrates the emission spectra of silicon dots synthesised with and without EDA, highlighting its role in optimizing fluorescence efficiency. This modification offers an innovative approach to tailoring silicon quantum dots for specific high-performance applications.

The fluorescence intensity of silicon quantum dots capped with EDA increased by approximately 4.5-fold compared to uncapped silicon quantum dots. Ethylenediamine (EDA) enhances the fluorescence intensity of silicon quantum dots (SiQDs) (Figure 4.1) through surface passivation, quantum confinement effects, and improved stability. EDA effectively reduces surface defects and dangling bonds that act as non-radiative recombination centres, allowing more efficient electron-hole recombination and, consequently, stronger fluorescence (Y. F. Wang et al., 2023). Additionally, the interaction between EDA and Sis can modify the electronic structure, potentially altering the energy bandgap and enhancing quantum yield. Furthermore, EDA functionalization improves the solubility and dispersion of silicon quantum dots in various solvents, preventing aggregation and ensuring consistent fluorescence performance(Shi et al., 2024).

The purpose of the experiment was to investigate the impact of EDA capping on the optical properties of silicon quantum dots, particularly their fluorescence intensity. By comparing capped and uncapped silicon quantum dots, the study aimed to confirm EDA's role in surface passivation, optimize synthesis conditions for enhanced

© COPYRIGHT UPM

fluorescence, and explore potential applications in bioimaging, sensing, and optoelectronics. This research provides valuable insights into surface chemistry modifications that can improve the photophysical properties of silicon quantum dots for advanced technological applications.

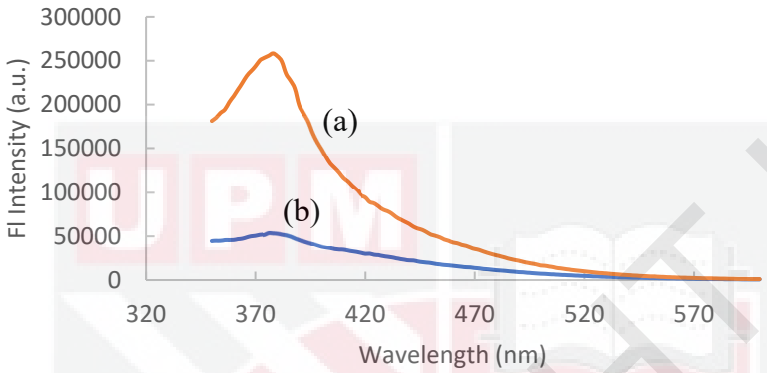

Figure 4.1: Emission spectra of SiQDs (a) SiQDs-EDA and (b) SiQDs without EDA

4.2 Characterization of as-prepared silicon quantum dots

4.2.1 UV/Vis and Fluorescent Spectroscopy

The optical properties of the produced silicon quantum dots were evaluated using UV–Vis and fluorescence spectrophotometers. The synthesized colloidal solution of silicon quantum dots, as demonstrated in Figure 4.2, exhibited a light-yellow transparent appearance under natural light. However, when exposed to a portable UV lamp, it emitted blue fluorescence (as shown in Figure 4.2c). This emission of blue fluorescence upon exposure to a UV lamp was also observed in a previous investigation (Liu et al., 2021b). The optical properties of silicon quantum dots were examined employing recording the UV-Vis spectrum, as depicted in Figure 4.2(a).

© COPYRIGHT UPM

This spectrum displays a continuous pattern of absorption within the range of 200 to 400 nm, with a noticeable peak occurring at approximately a wavelength of 329 nm. The silicon quantum dots exhibit a broad absorption band in the UV region, featuring two distinct absorption peaks at wavelengths of 250 and 350 nm. These peaks correspond to the π – p* and n – p* transitions of the silicon quantum dot, respectively. When subjected to UV light, the silicon quantum dots selectively absorb light at two specific wavelengths, namely 250 nm and 350 nm. These wavelengths correspond to different categories of electronic transitions. The π - p* transitions involve the elevation of electrons from π orbitals to p* orbitals, while the n - p* transitions entail the elevation of electrons from non-bonding orbitals to p* orbitals (Zhang et al., 2019). Another study identified a typical absorption band in the UV-Vis spectrum, marked by two absorption peaks observed at wavelengths of 280 nm and 350 nm (Eda et al., 2020).

The emission characteristics of silicon quantum dots are depicted in Figure 4.2(b). The highest emission peak of the silicon quantum dots observed at wavelength 382 nm was achieved when excited at wavelength 305 nm, which serves as the most optimal excitation wavelength for subsequent experimental investigations (Liu et al., 2022).

© COPYRIGHT UPM

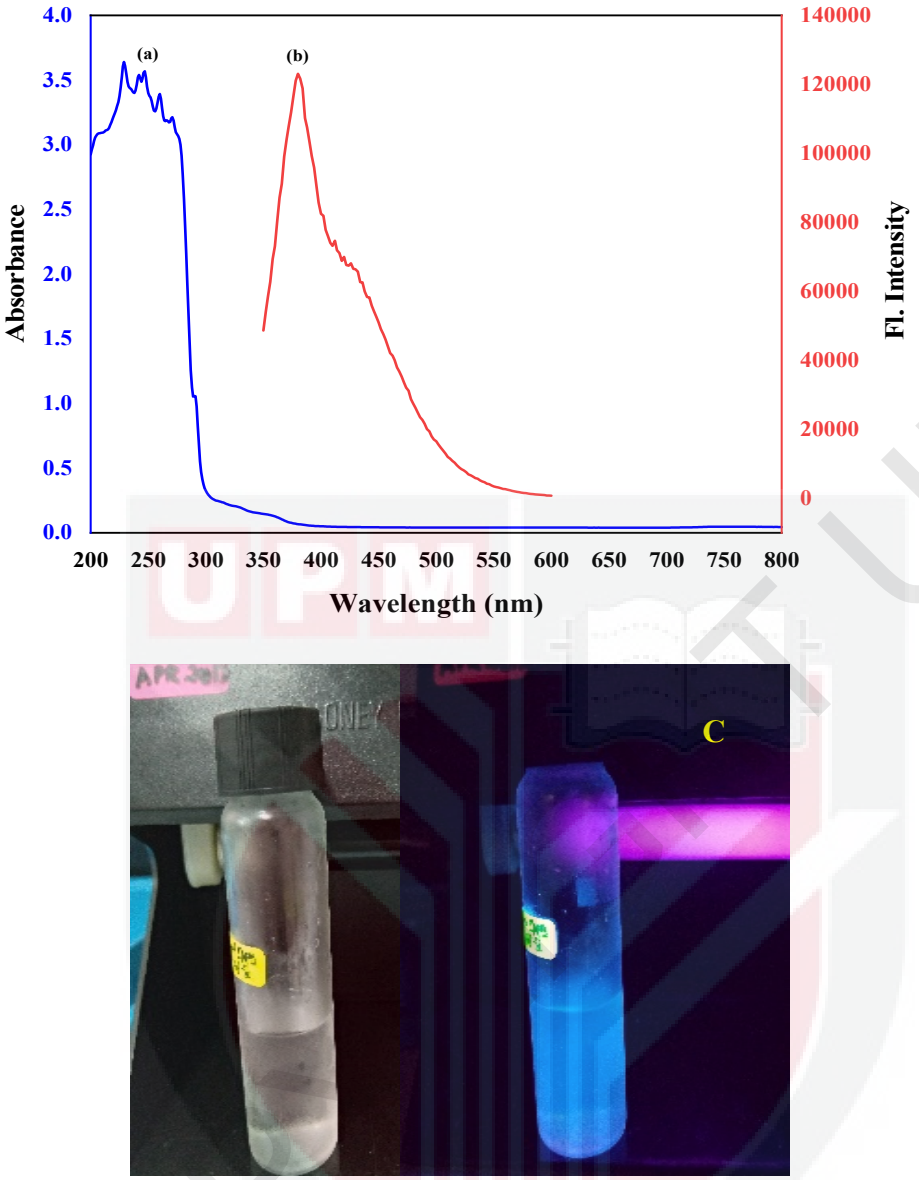

Figure 4.2: (a) UV/Vis spectrum of SiQDs, (b) Fluorescent emission of SiQDs, (c) SiQDs under natural light and UV lamp

4.2.2 Fourier-transform infrared spectroscopy (FTIR)

By using the Fourier Transform Infrared (FTIR) spectrum of silicon quantum dots, the surface groups and bonding composition of the material were investigated. As illustrated in Figure 4.3, silicon quantum dots C_1, containing a capping agent (EDA), and silicon quantum dots C_0 without a capping agent, exhibit a similar trend of spectrum. The similarity suggests that both types of silicon quantum dots have nearly

identical functional groups on their surfaces. The absorption peak at 3443 cm^{-1} was found as a result of the stretching vibrations of O-H, as shown in Figure 4.3 (Pan et al., 2022). The vibration of the C-N bond is responsible for the absorption peak found at 1301 cm^{-1}, whereas the unsaturated stretching vibration of the C-H bond is responsible for the peak detected at 2910 cm^{-1}. The stretching vibration of the C-O bond can be identified as the source of the signal at 1566 cm^{-1} (Liu et al., 2019). The Si-O bending vibrations, which were particularly notable, facilitated the successful preparation of silicon quantum dots. These vibrations were found to be the main cause of the significant absorbance observed at 1109 cm^{-1} and 1012 cm^{-1} (Miao et al., 2017). The findings indicated that the silicon quantum dot's surface exhibited a significant amount of hydroxyl and amino groups, which strongly suggested their superior water-holding properties. These results demonstrated the presence of multiple functional hydrophilic groups including amino and hydroxyl groups, on the silicon quantum dots surface, which strongly implied the silicon quantum dots' extraordinary water solubility.

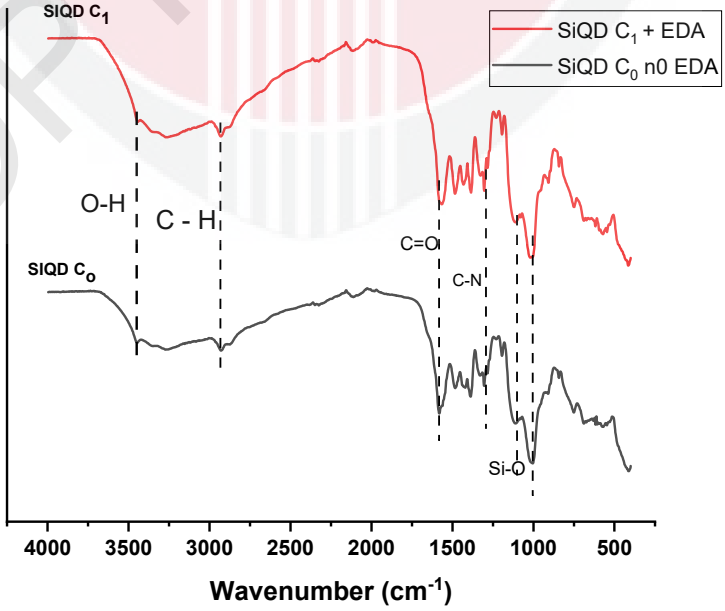

Figure 4.3: Fourier-transform infrared spectroscopy spectrum of SiQDs

© COPYRIGHT UPM

4.2.3 High-resolution Transmission electron microscope (HRTEM)

The majority of silicon quantum dots fell within the 11-12 nm size range (Upadhyay et al., 2022), with a narrow size distribution indicating uniformity in size. High-resolution transmission electron microscopy (HRTEM) images showed well-defined spherical structures of silicon quantum dots. The morphology and size distribution of the silicon quantum dots as depicted in Figure 4.4(a) exhibited pleasing uniformity, excellent dispersion, and a nearly spherical shape with sizes ranging from 10.5 nm to 12.95 nm. A prior study also reported that the prepared silicon quantum dots possessed a spherical shape and displayed a nearly uniform size distribution (Eda et al., 2020).

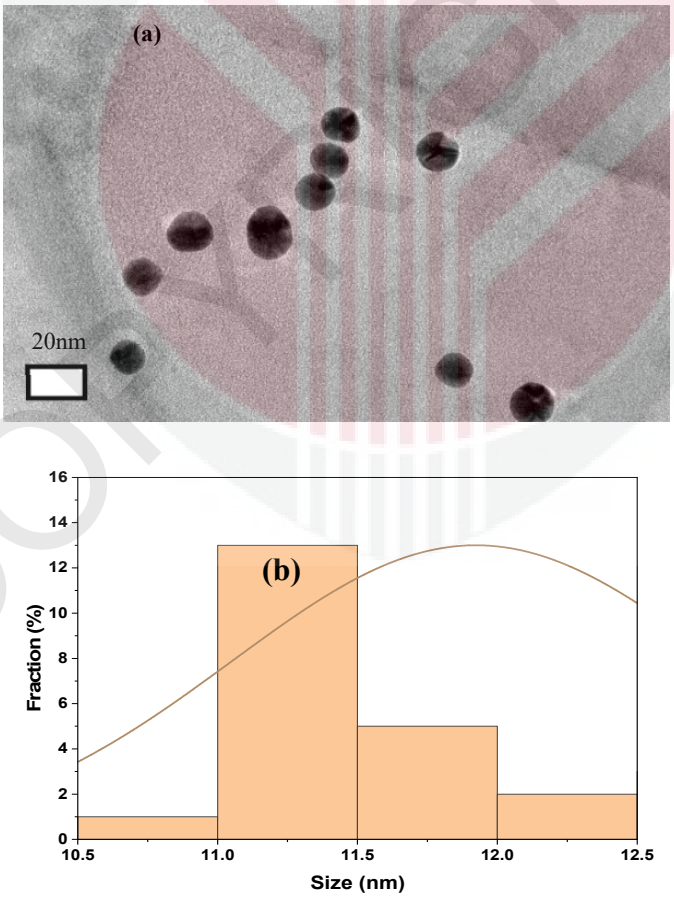

Figure 4.4: (a) shows HRTEM and pictures of SiQDs, and (b) the histogram size distribution of SiQDs at a 20 nm scale

4.2.4 X-ray diffraction (XRD)

X-ray diffraction (XRD) is a crucial method for examining silicon quantum dots offering comprehensive insights into their structural characteristics (Terada et al., 2020). The XRD pattern of the silicon quantum dots, showing a single broad peak at $2\theta = 21.05^{\circ}$, indicates that the material is predominantly amorphous (Figure 4.5). This peak corresponds to the short-range atomic order typical of amorphous silicon, as opposed to the well-defined lattice planes observed in crystalline silicon (Na et al., 2021; Capacity et al., 2019). The absence of additional peaks for planes such as {220} and {311} suggests a lack of long-range periodicity. This broad feature may also arise from the tiny size of the quantum dots (e.g., < 3 nm), where quantum confinement effects and surface states disrupt crystallinity (Holder & Schaak, 2019). Furthermore, the synthesis conditions, such as low-temperature processing or capping agents, might have inhibited the formation of well-crystallised domains. Overall, the XRD data suggests a predominantly disordered structure with possibly some local ordering, which can significantly impact the optical and electronic properties of the silicon quantum dots, such as enhancing quantum confinement effects or altering their bandgap (Bukhtiyarova, 2019).

© COPYRIGHT UPM

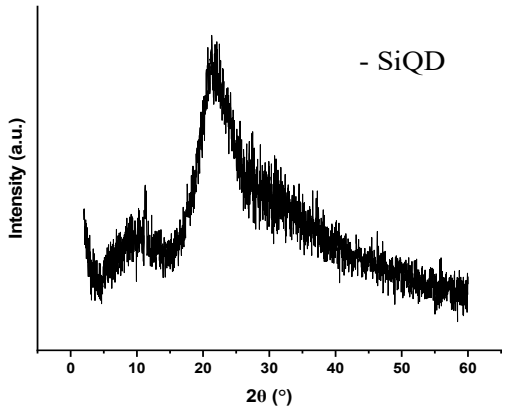

Figure 4.5: X-ray pattern of the prepared SiQDs

4.3 Silicon quantum dots for sensing application

The quenching process in silicon quantum dots (SiQDs) occurs when analytes like uric acid or glucose interact with the silicon quantum dots' surface or electronic structure. These interactions can lead to non-radiative energy or charge transfer, reducing fluorescence intensity through mechanisms such as Förster resonance energy transfer (FRET), photoinduced electron transfer (PET), or static quenching, depending on the analyte's proximity and nature (Noun et al., 2021; Liu et al., 2022). The extent of quenching is influenced by the silicon quantum dots' surface chemistry and the analyte's binding affinity, enabling sensitive detection based on fluorescence intensity changes (Xu et al., 2016).

The synthesis of silicon quantum dots from 3-aminopropyltrimethoxysilane (APTES), functionalised with ethylene diamine was prepared. The synthesised amino functionalised silicon quantum dots (NH_2@SiQDs) offer good water-solubility, high fluorescence quantum yield, and optical stability. A non-enzymatic assay of uric acid or glucose has been proposed based on the fluorescence quenching of NH_2@SiQDs in response to uric acid or glucose (Figure 4.6). It can be attributed to the fact that uric

© COPYRIGHT UPM

acid or glucose molecules linked the NH_2@SiQDs together via H-bonding and hydrophobic interactions that induced the self-aggregation of the silicon quantum dots and thus quenched the fluorescence. This quenching occurs because uric acid or glucose molecules interact with the amino groups (-NH_2) on the silicon quantum dots' surface, forming hydrogen bonds and hydrophobic interactions. These interactions induce self-aggregation of the silicon quantum dots, disrupting their surface states and electronic structures. The aggregation enhances non-radiative energy transfer mechanisms, reducing fluorescence emission. Consequently, the fluorescence intensity decreases proportionately to uric acid or glucose concentrations (Zhao et al., 2022).

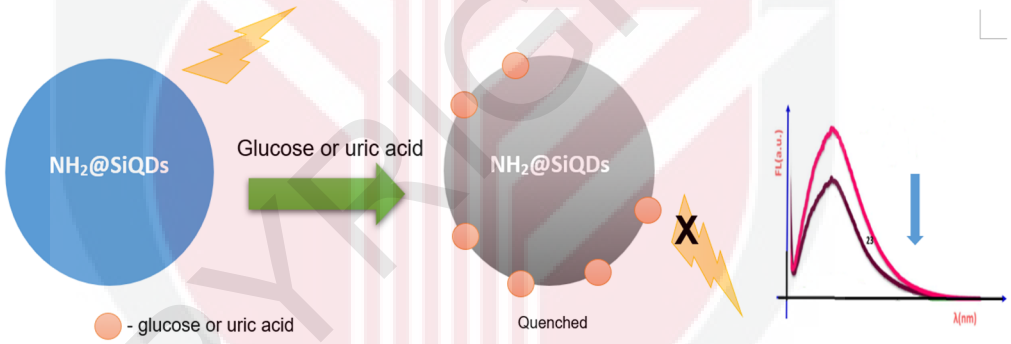

Figure 4.6: Schematic illustration of the NH_2@SiQDs for sensitive detection of uric acid and glucose

The measurement of net fluorescence quenching intensity is calculated according to the following equation (4.1):

$$\text{Net fluorescence quenching intensity } (\Delta \text{ Fl Intensity}) = F_o - F_i \qquad (4.1)$$

F_o = fluorescence intensity before the reaction (0 minute)

F_i = fluorescence intensity after the reaction (5 minutes for uric acid, and 15 minutes for glucose)

4.4 SiQDs for uric acid detection

a) Effect of pH buffer

Sodium phosphate buffer solutions with various pH values (7.0, 7.2, 7.4, 8.0, and 10) were employed in the optimisation process. Experimental conditions were optimised to improve the sensitivity of silicon quantum dots in a buffer system for uric acid detection. Given the substantial influence of the reaction solution's pH on the response system, the quenching effects of uric acid on the fluorescence intensity of silicon quantum dots were examined within a pH range of 7.0 to 10.0. Usually, uric acid detection is performed at pH 7.0 to 7.4 because it ensures the stability of the analytes and optimal surface interaction with the silicon quantum dots. At this pH, uric acid maintains its native molecular forms, and the silicon quantum dots' surface functional groups (e.g., carboxyl or hydroxyl) are appropriately ionised for efficient electrostatic and hydrogen bonding interactions, enabling sensitive and reliable detection in physiologically relevant conditions (Richette et al., 2010). As depicted in Figure 4.7, as the pH increased from 7.0 to 7.2 the net intensity also increased and above pH 7.2 the net intensity started to decrease. At pH 7.2, the silicon quantum dots' surface groups are in an optimal state, improving fluorescence (Films, 2019; Agarwal et al., 2023). Higher pH levels can deprotonate these groups, changing the surface charge and reducing fluorescence. Furthermore, increased pH can lead to more aggregation of silicon quantum dots, which also quenches fluorescence. Silicon quantum dots are more chemically stable at pH 7.2, while higher pH may cause reactions that reduce the fluorescence intensity. Lastly, the interaction between silicon quantum dots and uric

© COPYRIGHT UPM

acid is best at pH 7.2, enhancing fluorescence, whereas higher pH fades this interaction and decreases fluorescence (Agarwal et al., 2023).

As can be seen, the buffer indicates that the highest intensity (maximum peak 440 nm) is observed at a buffer with pH 7.2. Therefore, a buffer solution with pH 7.2 was chosen as the optimal pH for the detection of uric acid. Previous studies showed that the majority of the selected optimum pH values for uric acid determination fall within the range of 7.0 to 7.5 (Azmi et al., 2015; Zur & Des, 2008; Tatli et al., 2020).

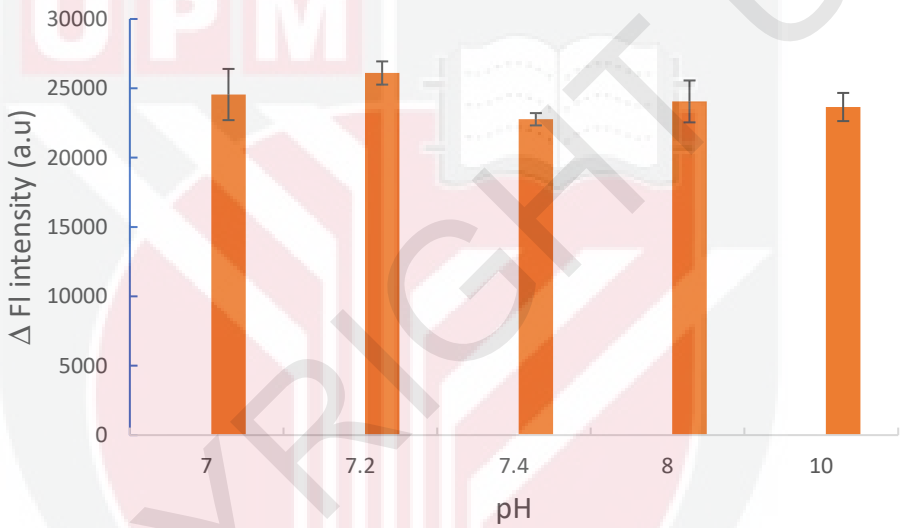

Figure 4.7: Effect of different pH buffer on the SiQDs response. The buffer consisting of 0.5 mg/ml of SiQDs and 0.6 mg/ml uric acid

b) Reaction time

Time plays a crucial role in various biochemical reactions, impacting their outcomes significantly. Consequently, Figure 4.8 depicts the intensity of the optimization of the desired silicon quantum dots system, and the uric solution conducted at various time intervals (0−30 min). As shown the reaction started immediately and the intensity reached its maximum at 5 minutes and started declining after 5 minutes of the reaction time. The most favourable outcome was attained within a 5-minute timeframe. The

© COPYRIGHT UPM

decline in sensor response after reaching the 5-minute maximum peak may be due to the saturation of binding sites on silicon quantum dots sensor. As the reaction progresses, the available sites for uric acid binding are occupied, reducing further interaction. Additionally, secondary processes like desorption, diffusion limitations, or degradation of the sensor or analyte could cause the signal to drop after the initial peak. Therefore, 5-minute reaction time was chosen for further study.

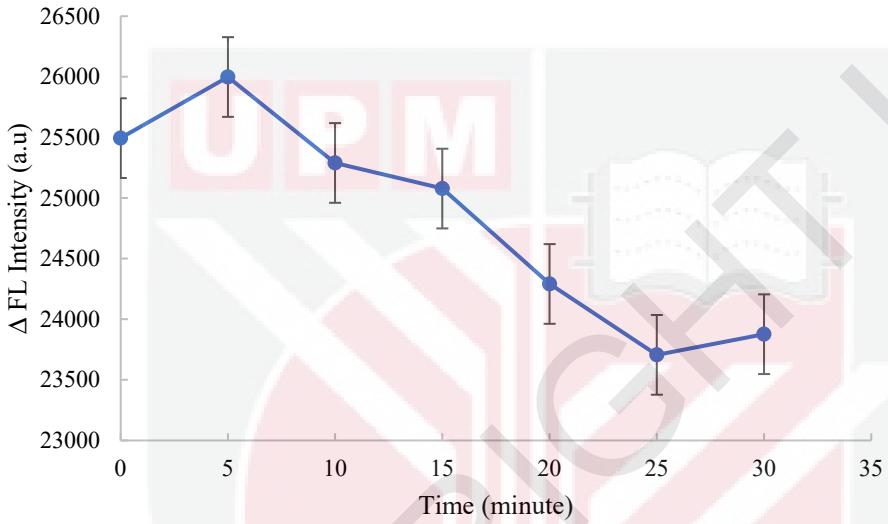

Figure 4.8: Influence of reaction time of 0.6 mg/ml uric acid interacts with 0.5 mg/ml SiQDs

4.4.1 Linearity study

The intensity of uric acid of different concentrations was measured with 0.5 mg/ml of silicon quantum dots in a phosphate buffer solution at pH 7.2. Figure 4.9 shows the dynamic response of the silicon quantum dots system when standard uric acid concentrations, ranging from 0.004 to 0.10 mg/ml, were introduced. As the uric acid concentration increased, the fluorescence intensity of the silicon quantum dots gradually decreased due to a quenching effect. A linear response within the uric acid concentration range of 0.004 – 0.100 mg/ml was observed (with a slope of y =233467*x*

© COPYRIGHT UPM

+ 3599.2, R^2 = 0.9829), with a calculated detection limit of 0.003 mg/ml and LOQ of 0.061 mg/ml. The obtained LOD was found to be lower than that reported by Zhou et al. (2024), which is 0.7 mg/mL for the detection of uric acid by surface-enhanced Raman spectroscopy, and higher than the LOD (0.05 mg/mL) reported by Wang et al., (2019) for the detection of uric acid by ratiometric fluorescence.

The detection range for uric acid (0.004–0.1 mg/mL) is selected based on its physiological relevance, clinical significance, and the capabilities of modern detection systems. Normal blood serum levels of uric acid typically range from 0.14 to 0.52 mg/mL, making it essential for sensors to detect lower concentrations in diluted samples or cases of hypouricemia. The chosen lower limit (0.004 mg/mL) ensures sensitivity to trace levels, while the upper limit (0.1 mg/mL) allows for early hyperuricemia detection before severe pathological conditions arise (Wen et al., 2024). These values align with biosensor technologies, including electrochemical and quantum-dot-based detection platforms, which can effectively measure nanomolar to micromolar concentrations. Additionally, the range accommodates different biological fluids such as blood, urine, and saliva, ensuring flexibility in clinical and point-of-care applications (Jovin & Mortlock, 2023).

© COPYRIGHT UPM

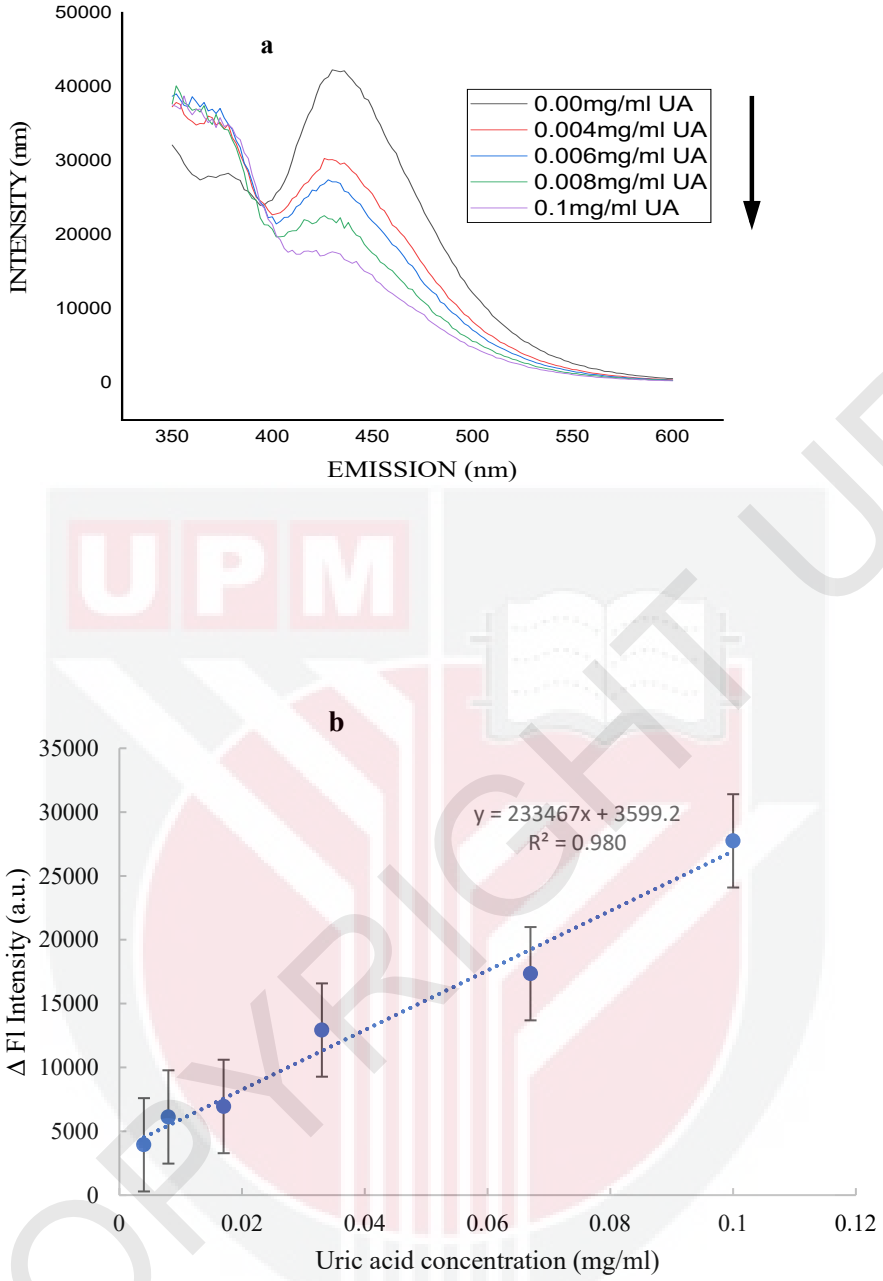

Figure 4.9: a) Fluorescence emission response of SiQDs in varying concentrations of uric acid, b) the calibration curve of uric acid concentration ranges from 0.004-0.100 mg/ml on SiQDs at pH 7.2

4.4.2 Real sample analysis

Table 4.1 presents the recovery of known concentrations of uric acid spiked in the urine sample. The table also shows the concentration of spiked uric acid in the urine

© COPYRIGHT UPM

sample was 0.05 mg/ml and 0.07 mg/ml, respectively. The recovery was calculated using the slope and intercept, accurately identifying the concentrations as 0.05 and 0.07 mg/ml. When 0.05 mg/ml and 0.07 mg/ml uric acid solutions were injected into 100-fold diluted urine, the recorded intensities indicated recoveries of 108.34% and 103.80%, respectively.

Table 4.1: Shows the recovery of the spiked uric concentrations in the urine sample
(n=3)

Sample	Added (mg/ml)	Found (mg/ml	% Recovery	% Error
Uric acid	0.00	ND	ND	ND
	0.05	0.054	108.34	8.0
	0.07	0.072	103.80	2.9

Note: ND – not detected

4.4.3 Interference study

The importance of biosensor selectivity cannot be overstated when working with actual biological samples. Therefore, investigating the selectivity of potential interfering substances is an essential part of sensor development. Several common substances typically found in urine were tested to evaluate their potential impact on the silicon quantum dot's ability to detect uric acid. The silicon quantum dots' fluorescence intensity changes were observed in the presence of interfering species. As shown in Table 4.2, there were positive responses regarding intensity changes for ascorbic acid, creatinine, glucose, urea, and KCl, while negative intensity change was observed for NaCl. Figure 4.10 depicts the bar chart of the fluorescence intensity of the interference species in the presence of uric acid. As can be noted from Table 4.2, the changes in the fluorescence intensity from all the interference species are within $100 \pm 5\%$.

© COPYRIGHT UPM

Interfering species in urine can greatly influence the detection of uric acid by either decreasing or increasing signal intensities. Signal reduction may arise from factors like competitive binding, quenching effects, or interactions with the urine matrix, where compounds such as sodium chloride or proteins inhibit the sensor's response (Martinez-Pérez et al., 2003; Li et al., 2021). Conversely, signal enhancement can occur due to overlapping signals from similar molecules (e.g., urea), synergistic effects, or contributions from optical active substances. These interferences may compromise the accuracy of uric acid measurements (Li et al., 2021). To mitigate such effects, approaches include employing highly selective sensors (e.g., nanozyme sensors), pre-treating samples to remove impurities, leveraging advanced signal processing techniques, or modifying sensor surfaces with materials like molecularly imprinted polymer (García-Vela, 2018).

Table 4.2: Assessment of potential interference in the actual urine sample (n = 3)

Interfering material	concentration (mg/ml)	Difference in fluorescence intensity of uric (%)
Ascorbic acid	0.2	3.8
Creatinine	0.2	3.4
Glucose	0.2	3.6
Urea	0.2	3.9
KCl	0.2	1.3
NaCl	0.2	-2.4

© COPYRIGHT UPM

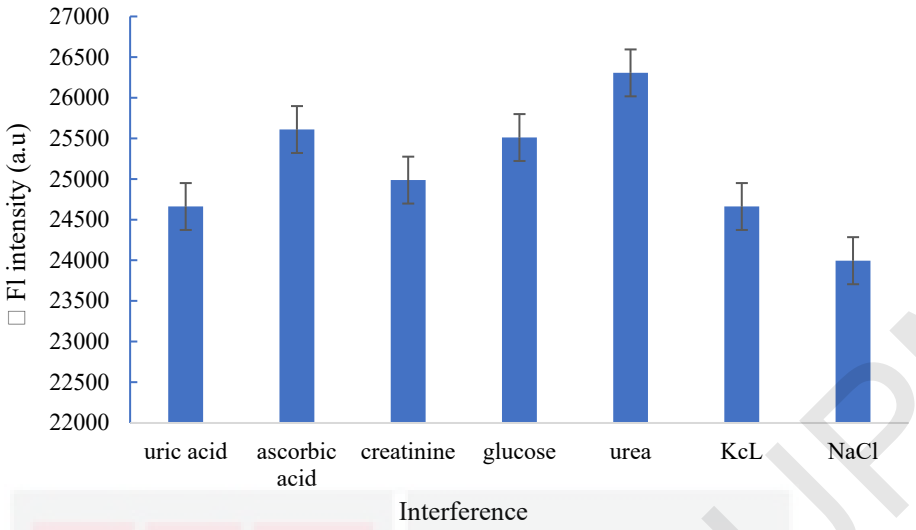

Figure 4.10: Evaluation of the potential interference in the sample

Reproducibility of uric acid study

The reproducibility of the prepared silicon quantum dots was examined with five different silicon quantum dots prepared independently to determine 0.03 mg/ml of uric acid. The relative standard deviation (RSD) obtained was 3.09 % (n = 5) for the prepared SiQDs which indicates a good reproducibility of the preparation of the sensors.

4.5 SiQDs for Glucose Detection

4.5.1 Optimization parameters

a) Determination of concentration of SiQDs

The determination of the concentration of the prepared silicon quantum dots is paramount for suitable application in the analysis. Among the tested concentrations, 0.5 mg/mL of the silicon quantum dots exhibited the highest fluorescence intensity.

© COPYRIGHT UPM

The concentration of silicon quantum dots is crucial for detecting uric acid or glucose because it affects the availability of reactive surface sites, the strength of optical signals, and analyte accessibility. At optimal concentration, silicon quantum dots provide sufficient interaction sites for analyte binding, generate measurable signal changes (e.g., fluorescence quenching or enhancement), and maintain a good signal-to-noise ratio. Too low concentration leads to weak signals, while too high can cause aggregation, self-quenching, or steric hindrance. Balancing these factors ensures efficient, sensitive, and reproducible detection of the analytes (Talyzin et al., 2019; Kim & Lee, 2023). At a concentration of silicon quantum dots of 0.5 mg/mL, it achieves optimal dispersion, allowing maximum interaction with the analyte without aggregation, which can quench fluorescence (Figure 4.11). This concentration also minimises self-absorption of emitted light while ensuring the surface of the silicon quantum dots is effectively utilised for analyte binding, leading to the highest fluorescence intensity. Therefore, it was selected and suitable for the application in the analysis.

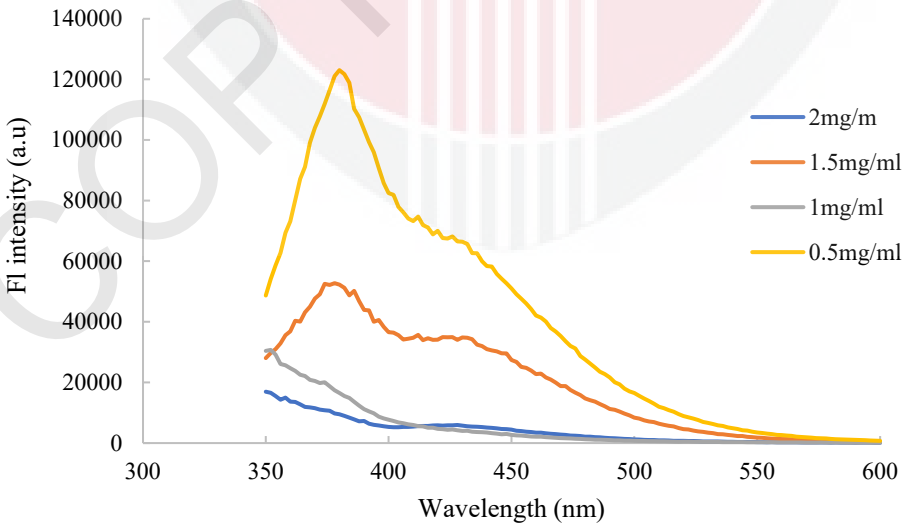

© COPYRIGHT UPM

Figure 4.11: Fluorescence spectra of SiQDs at different concentrations

b) Effect of pH buffer

Sodium phosphate buffer solutions at varying pH values (7.0, 7.2, 7.4, 8.0, and 8.5) were utilized in the optimization process. The experimental conditions were modified to enhance the sensitivity of silicon quantum dots in the buffer system for glucose detection. The considerable impact of the reaction solution's pH on the response system was investigated in the pH range of 7.0 to 8.5. As depicted in Figure 4.12, the intensity at different pH levels, using 1 mg/mL of glucose was measured at excitation/emission wavelengths of 350 nm / 440 nm. Analysis of the buffer indicates that the highest intensity is recorded at a pH of 7.2. Consequently, a buffer solution with a pH of 7.2 was identified as optimal for glucose detection. It is noteworthy that most of the selected optimal pH values for glucose determination fall within the range of 7.0 to 7.4 (Du et al., 2019; Mohammadifar et al., 2019; Ahmad et al., 2017; Wang & Lee, 2015).

The observed optimum pH of 7.2 for both uric acid and glucose detection can be attributed to several factors. This pH closely aligns with physiological conditions, ensuring compatibility with real biological samples such as blood and urine. Both analytes exhibit maximum stability and reactivity near neutral pH, minimizing ionization or degradation that could affect detection efficiency (Miranda & Aoyama, 2017). Additionally, silicon quantum dots (SiQDs) often perform optimally at neutral pH, where their surface properties remain stable, facilitating strong interactions with the analytes. Moreover, neutral pH minimizes interference from competing reactions

© COPYRIGHT UPM

or unstable substances in the sample, ensuring accurate and reliable detection (Dohnalová et al., 2014).

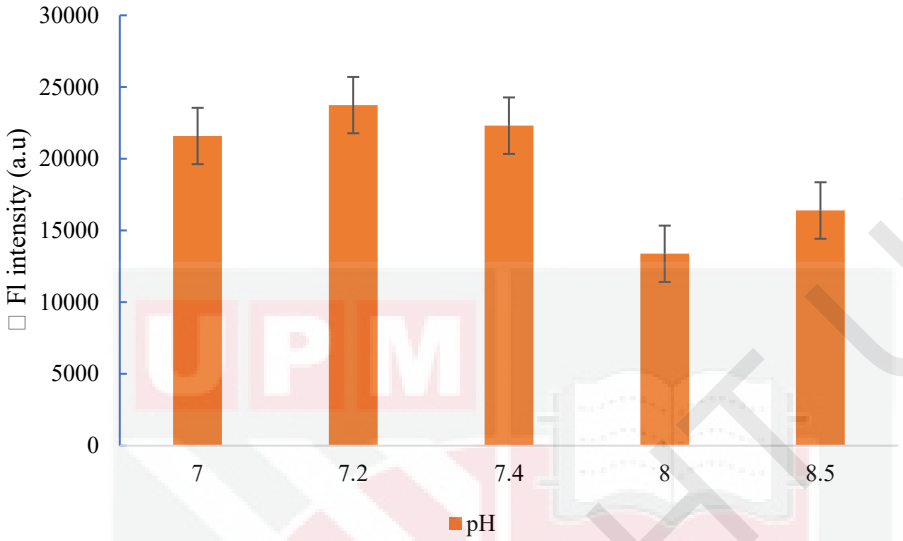

Figure 4.12: Effect of different pH buffers on SiQDs (0.5 mg/ml) response towards glucose (1 mg/ml)

c) Reaction time

Time is a critical factor in numerous biochemical reactions, greatly influencing their results. Therefore, we conducted optimization of the targeted biosensor (SiQDs) and the glucose solution at different time points. As depicted in Figure 4.14, the reaction commenced promptly, achieving peak intensity at the 15-minute mark, followed by a gradual decline thereafter. The optimal outcome was observed within a 15-minute window. The decline in fluorescence intensity of the silicon quantum dots sensor at 15 minutes may be due to saturation on the surface of the quantum dots. Additionally, interactions with glucose could saturate or alter the sensor's surface, affecting its optical properties. Aggregation of the quantum dots in the solution might also reduce their effective concentration, further diminishing fluorescence (Du et al., 2019).

© COPYRIGHT UPM

The slower response of the sensor towards glucose compared to uric acid (Figure 4.13 and 4.18) can be attributed to differences in their molecular structures (Faruk Hossain & Slaughter, 2021). This behaviour could be due to its larger size and more complex structure, which often necessitates specific multi-step enzymatic or catalytic interactions for oxidation or detection. This increases the response time (Faruk Hossain & Slaughter, 2021). On the other hand, uric acid has a simpler structure and is more readily oxidized under typical conditions, leading to a faster sensor response (Chittoor & Voruganti, 2019). Additionally, the diffusion rate of glucose molecules to the sensor's surface may be slower due to their larger size, further contributing to the delay. Variations in sensor surface affinity or catalytic efficiency towards each analyte could also play a role in the observed difference in response times (Beyer et al., 2014).

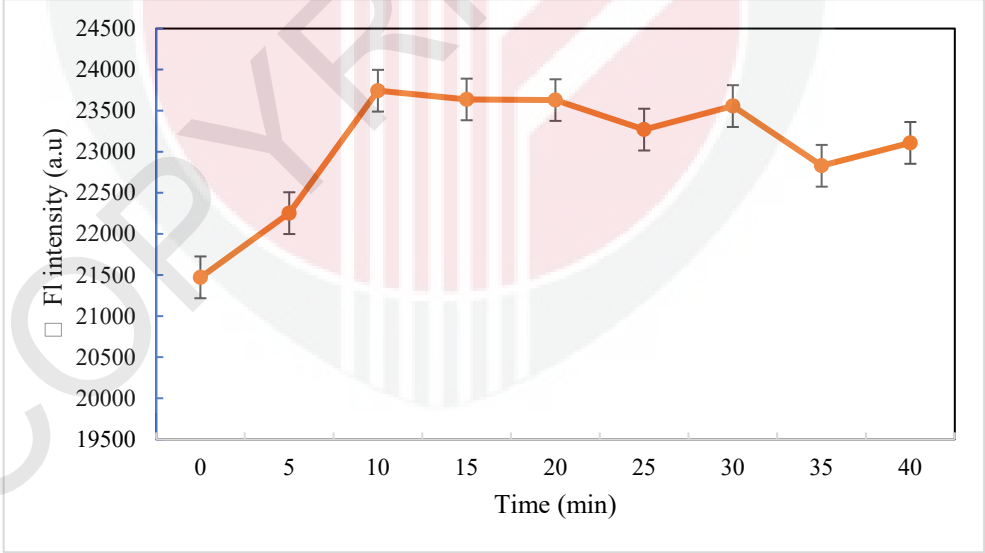

Figure 4.13: Influence of reaction time of SiQDs (0.5 mg/ml) with glucose (1 mg/ml) in PBS pH 7.2

4.5.2 Linearity study

© COPYRIGHT UPM

The effect of the silicon quantum dots system in phosphate buffer solution at pH 7.2 towards various glucose concentrations was investigated in this study. Figure 4.15 illustrates the dynamic response of the silicon quantum dots system when standard glucose concentrations ranging from 0.1 to 1.0 mg/ml were introduced. As the glucose concentration increased, there was a gradual reduction in the fluorescence intensity of the SiQDs due to their quenching effect. A linear relationship was observed within the glucose concentration range of 0.1 to 0.8 mg/ml (with a slope of y = 20249x - 1682.4, $R^2 = 0.9804$), the detection limit (LOD) was calculated to be 0.03 mg/ml and LOQ was 0.09 mg/ml slightly higher when compared to Du et al. (2019) findings in which the LOD was 0.002 mg/ml.

The glucose detection range (0.01–1 mg/mL) is designed to cover both normal and pathological conditions. Normal fasting blood glucose levels typically fall between 0.72 and 1.0 mg/mL, necessitating a sensor range that captures deviations indicative of hypoglycaemia and hyperglycaemia. The lower limit (0.01 mg/mL) allows for early hypoglycaemia detection, while the upper limit (1 mg/mL) ensures accurate monitoring of elevated glucose levels associated with diabetes (Tirosh et al., 2023). This range is well-matched to the sensitivity of advanced detection systems, including biosensors and nanomaterial-based platforms, which operate effectively within these concentration thresholds. Furthermore, the detection range supports measurements in diverse biological samples, including blood and interstitial fluids, ensuring adaptability for different diagnostic and monitoring needs (Jovin & Mortlock, 2023).

© COPYRIGHT UPM

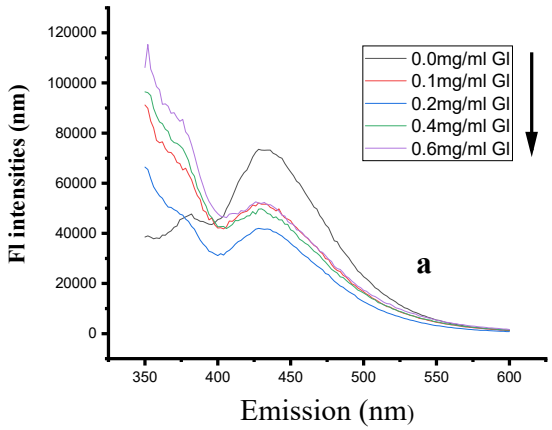

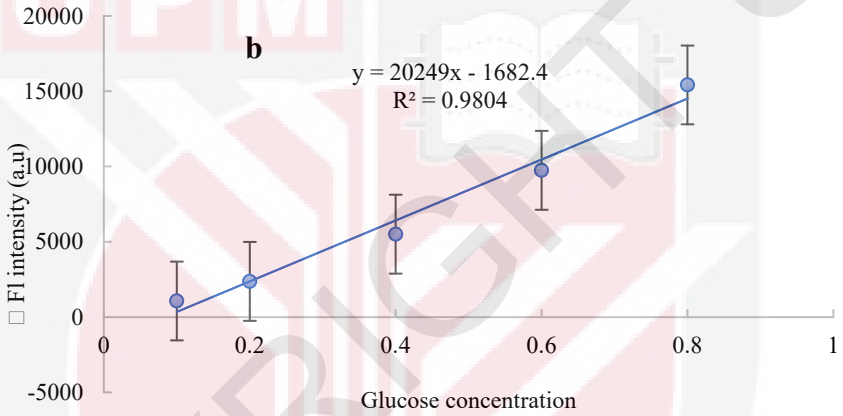

Figure 4.14: a) Fluorescence emission response of SiQDs in a phosphate buffer solution containing different concentrations of glucose, b) Calibration curve of glucose concentration in the range of 0.1 to 0.8 mg/ml in PBS pH 7.2 consisting of SiQDs (0.5 mg/ml)

4.5.3 Real sample analysis

Table 4.3 presents the recovery of an unknown concentration of mango juice after its reaction with 0.5 mg/ml of silicon quantum dots in phosphate buffer. Based on the slope and intercept from the standard curve (Figure 4.15), the concentration of unspiked mango juice with glucose was determined to be 0.161 mg/ml. The table also shows the concentrations of glucose spiked in the mango juice were 0.4 mg/ml and 0.6 mg/ml of glucose, respectively. The results show that the percentage of recoveries of

© COPYRIGHT UPM

glucose was in the range from 107.5% to 114.0%. This indicates that the silicon quantum dots sensor has great abilities to detect glucose in juice samples.

Table 4.3: shows the recovery of spiked glucose concentrations in mango juice (n = 5)

Sample	Added (mg/ml)	Found (mg/ml	% Recovery	% Error
Glucose	0.00	ND	ND	ND
	0.40	0.43	107.5	7.5
	0.60	0.68	114.0	13.3

Note: ND – not detected

4.5.4 Interference study

The significance of biosensor selectivity cannot be overstressed when handling real biological samples. Hence, it is crucial to investigate the selectivity of potential interfering substances as part of biosensor development. Various common substances typically found in glucose were analysed to gauge their potential impact on the biosensor's ability to detect glucose. Changes in biosensor fluorescence intensity were noted when these interfering species were present, using an emission wavelength of 440 nm. Table 4.4 demonstrates negative interference in terms of intensity changes from creatinine acid to ascorbic acid compounds, while Figure 4.16 illustrates the influence of the fluorescence response of glucose in the presence of interference species. Additionally, negative intensity changes were observed in urea and Na^+. According to the table, alterations in fluorescence intensity resulting from all interference species remain within 100 ± 5%.

Table 4.4: Assessment of potential interference in food sample (n=3)

Interfering substance	Concentration (mg/ml)	Change of fluorescence intensity (%)
Creatinine	0.2	-1.2
KCl	0.2	-2.3

© COPYRIGHT UPM

Ascorbic acid	0.2	-1.7
Urea	0.2	1.8
NaCl	0.2	1.6

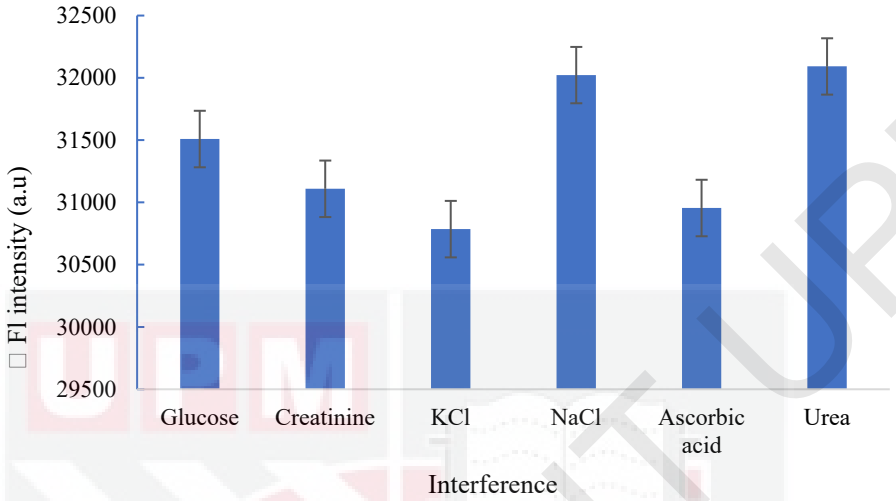

Figure 4.15: Influence of interference species for glucose determination using SiQDs system

4.5.5 Reproducibility of uric acid study

The reproducibility of the prepared silicon quantum dots was tested against 0.02 mg/ml of glucose using five different preparations. The relative standard deviation (RSD) obtained was 3.18% (n = 5) for the prepared silicon quantum dots, which indicates good reproducibility of the sensor preparation.

4.6 Performance Comparison of the SiQDs Sensor with the Others-based Sensor

The synthesised non-enzymatic fluorescence sensor based on silicon quantum dots (SiQDs) demonstrates remarkable efficiency in detecting uric acid and glucose, aligning with and even surpassing the performance of some previously reported sensors. In comparison to conventional enzymatic sensors, which suffer from stability

© COPYRIGHT UPM

issues due to enzyme degradation, the silicon quantum dots-based sensor offers enhanced longevity, consistent accuracy, and superior photostability.

Literature sources highlight the effectiveness of fluorescence-based approaches, particularly in their sensitivity and selectivity. For instance, Du et al. (2019) reported that fluorescent dyes, such as boronic acid derivatives, are commonly used in glucose detection due to their ability to form reversible covalent bonds with glucose hydroxyl groups. However, these organic dyes can suffer from photobleaching and require additional surface modifications for stability. In contrast, the hydrothermally synthesised silicon quantum dots used in this study exhibit higher quantum yield and greater photostability, making them a more robust alternative.

Studies on non-enzymatic sensors utilising metal oxides or organic dyes report good analytical performance, but they often require complex functionalisation or suffer from interference due to background fluorescence (Chen et al., 2018). For example, metal oxide-based sensors, such as Cu_2O and MnO_2, have been explored for glucose detection due to their electrocatalytic properties, yet they often exhibit interference from other electroactive species in biological fluids (Gao et al., 2021). In contrast, the silicon quantum dot-based sensor in this study eliminates the need for external catalysts while maintaining high selectivity and sensitivity.

Furthermore, Hassan et al. (2021) and Cao et al. (2023) emphasised that non-enzymatic fluorescence sensors have significant advantages over enzymatic approaches due to their resistance to environmental conditions such as temperature, pH, and humidity fluctuations. The synthesised silicon quantum dots in this work

© COPYRIGHT UPM

further extend these benefits by demonstrating enhanced biocompatibility and ease of functionalisation, as supported by prior research on silicon nanoparticles (Upadhyay et al., 2022).

© COPYRIGHT UPM

CHAPTER 5

CONCLUSION

5.1 Summary

In this study, a sensitive uric acid in urine and glucose in a food sample detection platform based on water-soluble silicon quantum dots has been developed successfully. Growing interest in uric acid sensors stems from the increasing global incidence of gout, caused by elevated uric acid levels in blood and urine. High uric acid levels can lead to serious health issues such as renal failure, heart disease, diabetes, hypertension, and stroke, making monitoring through blood and urine tests essential. Additionally, the rising prevalence of diabetes raises concerns for healthcare professionals, particularly concerning food security. Research has shown that functional foods can effectively manage diabetes by improving insulin sensitivity, reducing oxidative stress, and lowering blood glucose levels. Therefore, promoting these functional foods addresses diabetes management and food security by encouraging the availability of nutritious options while also managing uric acid levels for overall health.

5.2 Conclusion

Silicon quantum dots have been successfully prepared through a one-pot hydrothermal route. The synthesized silicon quantum dots were characterized using a fluorescence spectrophotometer which provides the optical properties of the silicon quantum dots.

© COPYRIGHT UPM

It exhibited a maximum emission peak at 382 nm when excited at 305 nm, and their surface morphology displayed satisfactory uniformity, appearing as near-spherical shapes ranging in size from 10.5 nm to 12.95 nm. Additionally, the X-ray diffraction determines the amorphous phase with only one peak at $2\theta = 21.05^{o}$ matching (111) plane for the silicon quantum dots.

The silicon quantum dots sensor allowed the detection of uric acid in the concentration range of 0.004 to 0.100 mg/ml with a limit of detection of 0.003 mg/ml, and glucose detection within the concentration range of 0.1 to 0.8 mg/ml, with a limit of detection of 0.03 mg/ml, respectively. This highlights its potential for use in healthcare and food quality control. The sensor's high sensitivity and selectivity allowed for accurate measurement of uric acid in body fluids and glucose in food. Its ability to detect both makes it useful for healthcare and industry, offering a simple, affordable, and reliable detection method.

5.3 Recommendation

There are some weaknesses of the research which should be highlight and improvised for further study. Based on this study the following recommendations are made:

1. Enhancement of Sensitivity and Selectivity

Future studies should focus on improving the selectivity of silicon quantum dot-based sensors by incorporating surface modifications with functional ligands or hybrid nanomaterials. The integration of metal nanoparticles, boronic acids, or molecular

© COPYRIGHT UPM

imprinting techniques could enhance binding specificity for uric acid and glucose, reducing interference from other biomolecules.

2. Stability and Long-Term Performance Optimization

Although silicon quantum dots exhibit excellent photostability, long-term sensor performance in diverse physiological and environmental conditions needs further evaluation. Research should investigate encapsulation techniques, such as polymer coatings or core-shell nanostructures, to enhance the stability of silicon quantum dots against oxidation and aggregation over prolonged use.

3. Real-time and Continuous Monitoring Systems

The development of real-time, continuous monitoring sensors is essential for applications in wearable and implantable devices. Future research should focus on integrating SiQDs-based fluorescence sensors into flexible electronic platforms, microfluidic systems, and smartphone-compatible biosensors for non-invasive glucose and uric acid monitoring in sweat, saliva, or interstitial fluid.

4. Expansion of Detection Methods and Multiplex Sensing

Exploring multi-analyte detection capabilities is crucial for diagnosing and monitoring metabolic disorders. Future sensors should be designed to simultaneously detect multiple biomarkers, such as glucose, uric acid, and lactate, using ratiometric fluorescence or Förster resonance energy transfer (FRET)-based mechanisms. This advancement would enable comprehensive health monitoring from a single sample.

© COPYRIGHT UPM

5. Eco-Friendly and Scalable Synthesis Approaches

The hydrothermal synthesis of silicon quantum dots presents an eco-friendly and cost-effective alternative to traditional methods. However, large-scale production with consistent quality and controlled particle size distribution remains a challenge. Future work should optimize synthesis conditions, explore green chemistry approaches, and develop scalable fabrication techniques to facilitate commercial viability.

© COPYRIGHT UPM

REFERENCES

Agarwal, K., Rai, H., & Mondal, S. (2023). Quantum dots: an overview of synthesis, properties, and applications. *Materials Research Express*, *10*(6). p.123-128

Aggas, J. R., Sánchez-Sinencio, E., & Guiseppi-Elie, A. (2020). Wien Oscillator Using Organic Enzyme-Chemiresistors for Fused Measurement of Glucose and Lactate. *Advanced Intelligent Systems*, *2*(7), 223-231

Ahmad, I. author. (2017). *Non-invasive quantum dot based sensors for the detection of glucose and cholesterol in saliva*. 15-20

Alwis, U. S., Haddad, R., Monaghan, T. F., Abrams, P., Dmochowski, R., Bower, W., Wein, A. J., Roggeman, S., Weiss, J. P., Mourad, S., Delanghe, J., & Everaert, K. (2020). Impact of food and drinks on urine production: A systematic review. *International Journal of Clinical Practice*, *74*(9). (76-81)

Askari, S., Macias-Montero, M., Velusamy, T., Maguire, P., Svrcek, V., & Mariotti, D. (2022). Silicon-based quantum dots: Synthesis, surface and composition tuning with atmospheric pressure plasmas. *Journal of Physics D: Applied Physics*, *48*(31),18-22

Azmi, N. E., Ramli, N. I., Abdullah, J., Abdul Hamid, M. A., Sidek, H., Abd Rahman, S., Ariffin, N., & Yusof, N. A. (2015). A simple and sensitive fluorescence based biosensor for the determination of uric acid using H2O2-sensitive quantum dots/dual enzymes. *Biosensors and Bioelectronics*, *67*, 129–133.

Azmi, N. E., Rashid, A. H. A., Abdullah, J., Yusof, N. A., & Sidek, H. (2018). Fluorescence biosensor based on encapsulated quantum dots/enzymes/sol-gel for non-invasive detection of uric acid. *Journal of Luminescence*, *202*, 309–315.

Baig, N., Kawde, A. N., & Elgamouz, A. (2022). A cost-effective disposable graphene-based sensor for sensitive and selective detection of uric acid in human urine. *Biosensors and Bioelectronics: X*, *11*(May), 100205.

Bera, D., Qian, L., Tseng, T. K., & Holloway, P. H. (2010). Quantum dots and their multimodal applications: A review. *Materials*, *3*(4), 2260–2345.

Beyer, U., Wyss, T., Robin, F., & Heinemann, L. (2014). Glucose measurement by affinity sensor and pulsed measurements of fluidic resistances: Proof of principle. *Journal of Diabetes Science and Technology*, *8*(1), 100–108.

Bobulescu, I. A., & Moe, O. W. (2012). Renal Transport of Uric Acid: Evolving Concepts and Uncertainties. *Advances in Chronic Kidney Disease*, *19*(6), 358–371.

Bukhtiyarova, M. V. (2019). A review on effect of synthesis conditions on the formation of layered double hydroxides. *Journal of Solid State Chemistry*, *269*(October 2018), 494–506.

© COPYRIGHT UPM

Cao, W., Guo, T., Ding, Y., Hu, Y., & Liu, D. (2023). Substantially boosting the performance of non-enzymatic glucose sensing: Introducing a novel CuS nanosheet anchored on hollow Ni(OH)2 nanosphere. *Applied Surface Science*, *634*(May), 157650.

Capacity, E. D., Phuong, L., Tran, P., Thuy, N., Le, T., & Cao, M. (2019). *The Engineering of Porous Silica and Hollow Silica*. 1–11.

Cells, K., Blodgett, A. B., & Kamyshko, I. (2011). *Original Article A Fluorescence Method for Measurement of Glucose*. *13*(7), 1245-1272

Chen, C., Zhang, Y., Zhang, Z., He, R., & Chen, Y. (2018). Fluorescent Determination of Glucose Using Silicon Nanodots. *Analytical Letters*, *51*(18), 2895–2905.

Chevinsky, J. R., Lee, S. H., Blanck, H. M., & Park, S. (2021). Prevalence of Self-Reported Intake of Sugar-Sweetened Beverages Among US Adults in 50 States and the District of Columbia, 2010 and 2015. *Preventing Chronic Disease*, *18*, E35.

Chittoor, G., & Voruganti, V. S. (2019). Hyperuricemia and gout. In *Principles of Nutrigenetics and Nutrigenomics: Fundamentals of Individualized Nutrition*. Elsevier Inc. https://doi.org/10.1016/B978-0-12-804572-5.00053-7

Croissant, J. G., Fatieiev, Y., & Khashab, N. M. (2017). Degradability and Clearance of Silicon, Organosilica, Silsesquioxane, Silica Mixed Oxide, and Mesoporous Silica Nanoparticles. *Advanced Materials*, *29*(9), 230-141

Dehlin, M., Jacobsson, L., & Roddy, E. (2020). Global epidemiology of gout: prevalence, incidence, treatment patterns and risk factors. *Nature Reviews Rheumatology*, *16*(7), 380–390.

Dohnalová, K., Gregorkiewicz, T., & Kůsová, K. (2014). Silicon quantum dots: Surface matters. *Journal of Physics Condensed Matter*, *26*(17), 675-681

Du, L., Li, Z., Yao, J., Wen, G., Dong, C., & Li, H. W. (2019). Enzyme free glucose sensing by amino-functionalized silicon quantum dot. *Spectrochimica Acta - Part A: Molecular and Biomolecular Spectroscopy*, *216*, 303–309.

Eda, H., Kara, Ş., DemİrhanB., & DemİrhanB. E. R. (2020). *Highly luminescent water-dispersed silicon quantum dots for fluorometric determination of oxytetracycline in milk samples*. *November 2019*, 1713–1722.

El Ridi, R., & Tallima, H. (2017). Physiological functions and pathogenic potential of uric acid: A review. *Journal of Advanced Research*, *8*(5), 487–493.

Elsayed, N. A., Aleppo, G., Aroda, V. R., Bannuru, R. R., Brown, F. M., Bruemmer, D., Collins, B. S., Hilliard, M. E., Isaacs, D., Johnson, E. L., Kahan, S., Khunti, K., Leon, J., Lyons, S. K., Perry, M. Lou, Prahalad, P., Pratley, R. E., Seley, J. J., Stanton, R. C., … Gabbay, R. A. (2023). 5. Facilitating Positive Health Behaviors and Well-being to Improve Health Outcomes: Standards of Care in Diabetes—2023. *Diabetes Care*, *46*(January), S68–S96.

© COPYRIGHT UPM

Faruk Hossain, M., & Slaughter, G. (2021). Flexible electrochemical uric acid and glucose biosensor. *Bioelectrochemistry*, *141*, 107870.

Fava, E. L., Silva, T. A., Martimiano, T., Moraes, F. C. De, Faria, R. C., & Fatibello-filho, O. (2019). AC SC. *987-991*

Feng, X., Zheng, Y., Guan, H., Zhou, X., Xu, Y., Zhang, X., Fu, C., Xiao, J., & Ye, Z. (2021). The Association between Urinary Glucose and Renal Uric Acid Excretion in Non-diabetic Patients with Stage 1-2 Chronic Kidney Disease. *Endocrine Research*, *46*(1), 28–36.

Films, N. B. (2019). *Quantum Dots Modified Sodium*.

Galant, A. L., Kaufman, R. C., & Wilson, J. D. (2020). Glucose : Detection and analysis q. *Food Chemistry*, *188*, 149–160.

Gao, G., Jiang, Y. W., Jia, H. R., Yang, J., & Wu, F. G. (2018). On-off-on fluorescent nanosensor for Fe3+ detection and cancer/normal cell differentiation via silicon-doped carbon quantum dots. *Carbon*, *134*, 232–243.

Gao, J., Huang, W., Chen, Z., Yi, C., & Jiang, L. (2019). Sensors and Actuators B : Chemical Simultaneous detection of glucose , uric acid and cholesterol using fl exible microneedle electrode array-based biosensor and multi-channel portable electrochemical analyzer. *Sensors & Actuators: B. Chemical*, *287*(January), 102–110.

Gao, W., Zhou, X., Heinig, N. F., Thomas, J. P., Zhang, L., & Leung, K. T. (2021). Nonenzymatic Saliva-Range Glucose Sensing Using Electrodeposited Cuprous Oxide Nanocubes on a Graphene Strip. *ACS Applied Nano Materials*, *4*(5), 4790–4799.

García-Vela, A. (2018). Unravelling the mechanisms of interference between overlapping resonances. *Physical Chemistry Chemical Physics*, *20*(6), 3882–3887.

Geng, X., Li, Z., Hu, Y., Liu, H., Sun, Y., Meng, H., Wang, Y., Qu, L., & Lin, Y. (2018). One-Pot Green Synthesis of Ultrabright N-Doped Fluorescent Silicon Nanoparticles for Cellular Imaging by Using Ethylenediaminetetraacetic Acid Disodium Salt as an Effective Reductant [Research-article]. *ACS Applied Materials and Interfaces*, *10*(33), 27979–27986.

Gerdan, Z., Saylan, Y., & Denizli, A. (2022). Recent Advances of Optical Sensors for Copper Ion Detection. *Micromachines*, *13*(8), 754-756

Guan, W., Duan, X., & Reed, M. A. (2014). Highly specific and sensitive non-enzymatic determination of uric acid in serum and urine by extended gate field effect transistor sensors. *Biosensors and Bioelectronics*, *51*, 225–231.

Guo, J. (2016). Uric acid monitoring with a smartphone as the electrochemical analyzer. *Analytical Chemistry*, *88*(24), 11986–11989.

© COPYRIGHT UPM

Guo, J., & Ma, X. (2017). Simultaneous monitoring of glucose and uric acid on a single test strip with dual channels. *Biosensors and Bioelectronics*, *94*, 415–419.

Guo, Y., Huang, Z., Sang, D., Gao, Q., & Li, Q. (2020). *The Role of Nutrition in the Prevention and Intervention of Type 2 Diabetes*. *8*(September), 1–15.

Hassan, M. H., Vyas, C., Grieve, B., & Bartolo, P. (2021). Recent advances in enzymatic and non-enzymatic electrochemical glucose sensing. *Sensors*, *21*(14).

Holder, C. F., & Schaak, R. E. (2019). Tutorial on Powder X-ray Diffraction for Characterizing Nanoscale Materials. *ACS Nano*, *13*(7), 7359–7365.

Huang, X. C., Inoue-Aono, Y., Moriyasu, Y., Hsieh, P. Y., Tu, W. M., Hsiao, S. C., Jane, W. N., & Hsu, H. Y. (2016). Plant Cell Wall-Penetrable, Redox-Responsive Silica Nanoprobe for the Imaging of Starvation-Induced Vesicle Trafficking. *Analytical Chemistry*, *88*(20), 10231–10236.

Huang, Y., Li, P., Zhao, R., Zhao, L., Liu, J., Peng, S., Fu, X., Wang, X., Luo, R., Wang, R., & Zhang, Z. (2022). Silica nanoparticles: Biomedical applications and toxicity. *Biomedicine and Pharmacotherapy*, *151*(April), 113053.

Igathinathane, C., Pordesimo, L. O., Columbus, E. P., Batchelor, W. D., & Methuku, S. R. (2008). Shape identification and particles size distribution from basic shape parameters using ImageJ. *Computers and Electronics in Agriculture*, *63*(2), 168–182.

Jamnik, J., Rehman, S., Blanco Mejia, S., De Souza, R. J., Khan, T. A., Leiter, L. A., Wolever, T. M. S., Kendall, C. W. C., Jenkins, D. J. A., & Sievenpiper, J. L. (2022). Fructose intake and risk of gout and hyperuricemia: A systematic review and meta-analysis of prospective cohort studies. *BMJ Open*, *6*(10). 487-490

Jarnda, K. V., Wang, D., Qurrat-Ul-Ain, Anaman, R., Johnson, V. E., Roberts, G. P., Johnson, P. S., Jallawide, B. W., Kai, T., & Ding, P. (2023). Recent advances in electrochemical non-enzymatic glucose sensor for the detection of glucose in tears and saliva: A Review. *Sensors and Actuators A: Physical*, *363*(July), 114778.

Joshi, A., & Slaughter, G. (2025). Electrochemical carbon-based sensors for non-enzymatic uric acid sensing. *Microchemical Journal*, *208*(July 2024), 112331.

Jovin, D. G., & Mortlock, R. (2023). *Daniel G. Jovin * and Ryland Mortlock *. 96*, 1–2.

Kayode, A. A. A., Adebodun, G. O., Fabunmi, D. I., & Kayode, O. T. (2023). *Role of functional foods in the management of diabetes mellitus : a concise review*. *2*(7), 29–42.

Kerian, K., & State, K. (2023). *Carbon Quantum Dots Coupled Au Nanoparticle as Fluorescence-Based DNA Biosensors For Dengue Virus Detection*. *52*(11), 3307–3323.

© COPYRIGHT UPM

Kim, E. J., Kim, E. B., Lee, S. W., Cheon, S. A., Kim, H. J., Lee, J., Lee, M. K., Ko, S., & Park, T. J. (2017). An easy and sensitive sandwich assay for detection of Mycobacterium tuberculosis Ag85B antigen using quantum dots and gold nanorods. *Biosensors and Bioelectronics*, *87*, 150–156.

Kim, T., & Lee, J. (2023). Silicon nanoparticles: fabrication, characterization, application and perspectives. *Micro and Nano Systems Letters*, *11*(1).

Kim, Y., Jeon, Y., Na, M., Hwang, S. J., & Yoon, Y. (2024). Recent Trends in Chemical Sensors for Detecting Toxic Materials. *Sensors*, *24*(2), 21-26

Kristensen, K. B., Ranjan, A. G., McCarthy, O. M., Bracken, R. M., Nørgaard, K., & Schmidt, S. (2024). Sensor-Based Glucose Metrics during Different Diet Compositions in Type 1 Diabetes—A Randomized One-Week Crossover Trial. *Nutrients*, *16*(2), 1–12.

Kumar, A., Khandelwal, M., Gupta, S. K., Kumar, V., & Rani, R. (2019). Fourier transform infrared spectroscopy: Data interpretation and applications in structure elucidation and analysis of small molecules and nanostructures. In *Data Processing Handbook for Complex Biological Data Sources*. Elsevier Inc. 1238-1241

Kumari, C., Sain, D., & Dey, S. (2018). Highly selective and safe 'in vitro' detection of biologically important 'Uric acid' in living cells by a new fluorescent 'turn-on' probe along with quantum chemical calculation. *Sensors and Actuators, B: Chemical*, *264*, 208–215.

Lepowsky, E., Ghaderinezhad, F., Knowlton, S., Tasoglu, S., Lepowsky, E., Ghaderinezhad, F., & Knowlton, S. (2017). *Paper-based assays for urine analysis Paper-based assays for urine analysis*. *051501*.

Li, F., He, T., Wu, S., Peng, Z., Qiu, P., & Tang, X. (2021). Visual and colorimetric detection of uric acid in human serum and urine using chitosan stabilized gold nanoparticles. *Microchemical Journal*, *164*(November 2020), 105987.

Li, W., Liu, D., Dong, D., & You, T. (2021). Microwave-assisted synthesis of fluorescent silicon quantum dots for ratiometric sensing of Hg (II) based on the regulation of energy transfer. *Talanta*, *226*(September 2020), 122093.

Li, X., Chen, G., Hu, A., Xiong, Y., Yang, T., Ma, C., Li, L., Gao, H., Zhu, C., Wu, Y., Gu, J., Wu, H., Zhou, Y., Guan, W., & Zhang, W. (2024). Non-enzymatic Detection of Uric Acid in Serum and Urine by Fluorescent and Visual Dual-Mode Sensor Based on 3-aminophenylboric Acid Functionalized Carbon Dots. *Journal of Fluorescence*.

Li, Y., Li, W., Zhang, H., Liu, Y., Ma, L., & Lei, B. (2020). Amplified light harvesting for enhancing Italian lettuce photosynthesis using water soluble silicon quantum dots as artificial antennas. *Nanoscale*, *12*(1), 155–166.

© COPYRIGHT UPM

Li, Y., Zhang, H., Yao, Y., Gong, T., Dong, R., Li, D., Liu, Y., & Lei, B. (2020). Promoted off-on recognition of H2O2 based on the fluorescence of silicon quantum dots assembled two-dimensional PEG-MnO2 nanosheets hybrid nanoprobe. *Microchimica Acta*, *187*(6), 188-190

Liu, J., Geng, Z., Fan, Z., Liu, J., & Chen, H. (2019). Point-of-care testing based on smartphone: The current state-of-the-art (2017–2018). *Biosensors and Bioelectronics*, *132*(January), 17–37.

Liu, Y., Cao, L., Zan, M., Peng, J., Wang, P., Pang, X., Zhang, Y., Li, L., Dong, W. F., & Mei, Q. (2021a). Cyan-emitting silicon quantum dots as a fluorescent probe directly used for highly sensitive and selective detection of chlorogenic acid. *Talanta*, *233*(April). 122465-122469

Liu, Y., Cao, L., Zan, M., Peng, J., Wang, P., Pang, X., Zhang, Y., Li, L., Dong, W. F., & Mei, Q. (2021b). Cyan-emitting silicon quantum dots as a fluorescent probe directly used for highly sensitive and selective detection of chlorogenic acid. *Talanta*, *233*. 122465

Liu, Y., Li, W., Wu, P., Ma, C., Wu, X., Xu, M., Luo, S., Xu, Z., & Liu, S. (2019). Hydrothermal synthesis of nitrogen and boron co-doped carbon quantum dots for application in acetone and dopamine sensors and multicolor cellular imaging. *Sensors and Actuators, B: Chemical*, *281*(July 2018), 34–43.

Liu, Y., Zan, M., Cao, L., Peng, J., Wang, P., & Pang, X. (2022). *F-doped silicon quantum dots as a novel fluorescence nanosensor for quantitative detection of new coccine and application in food samples*. *179*(March).

Lopes, F. M., Batista, K. de A., Batista, G. L. A., & Fernandes, K. F. (2021). Biossensor para determinação de glicose em amostras reais de bebidas. *Ciencia e Tecnologia de Alimentos*, *32*(1), 65–69.

Lu, Q., Chen, X., Liu, D., Wu, C., Liu, M., Li, H., Zhang, Y., & Yao, S. (2019). A turn-on fluorescent probe for vitamin C based on the use of a silicon/CoOOH nanoparticle system. *Microchimica Acta*, *186*(2), 1–8.

Luka, G., Ahmadi, A., Najjaran, H., Alocilja, E., Derosa, M., Wolthers, K., Malki, A., Aziz, H., Althani, A., & Hoorfar, M. (2015). Microfluidics integrated biosensors: A leading technology towards lab-on-A-chip and sensing applications. *Sensors (Switzerland)*, *15*(12), 30011–30031.

Ma, C., Jiang, N., Sun, X., Kong, L., Liang, T., Wei, X., & Wang, P. (2023). Progress in optical sensors-based uric acid detection. *Biosensors and Bioelectronics*, *237*(July), 115495.

Maahs, D. M., & Clements, M. A. (2020). *within the T1D Exchange*. 217–228.

Martinez-Pérez, D., Ferrer, M. L., & Mateo, C. R. (2003). A reagent less fluorescent sol-gel biosensor for uric acid detection in biological fluids. *Analytical Biochemistry*, *322*(2), 238–242.

© COPYRIGHT UPM

Martirosyan, D. M., & Singh, J. (2015). A new definition of functional food by FFC: What makes a new definition unique? *Functional Foods in Health and Disease*, *5*(6), 209–223.

Matea, C. T., Mocan, T., Tabaran, F., Pop, T., Mosteanu, O., Puia, C., Iancu, C., & Mocan, L. (2017). Quantum dots in imaging, drug delivery and sensor applications. *International Journal of Nanomedicine*, *12*, 5421–5431.

Matsinkou Soh, R., Ngaha Damndja, W., & Njintang Yanou, N. (2024). Functional foods of sub-Saharan Africa and their implications in the management of type 2 diabetes: A review. *Food Science and Nutrition*, *12*(1), 24–34.

Miao, X., Yan, X., Qu, D., Li, D., Tao, F. F., & Sun, Z. (2017). Red Emissive Sulfur, Nitrogen Codoped Carbon Dots and Their Application in Ion Detection and Theraonostics. *ACS Applied Materials and Interfaces*, *9*(22), 18549–18556.

Miranda, M. A., & Aoyama, H. (2017). Enzymes with Two Optimum pH Values. *World Journal of Research and Review*, *5*, 5–11.

Mohamed, Y. A., & Higazi, S. E. (2016). *Research Article Determination of Sugar in Cane Juices using High Performance Liquid Chromatography HPLC and Ultra violet UV at Kenana Sugar Factory – Sudan*. *8*(12), 71–75.

Mohammadifar, M., Tahernia, M., & Choi, S. (2019). *An Equipment-Free , Paper-Based Electrochemical Sensor for Visual Monitoring of Glucose Levels in Urine*. 2894-2899

Montalti, M., Prodi, L., Rampazzo, E., & Zaccheroni, N. (2014). *Chem Soc Rev Dye-doped silica nanoparticles as luminescent organized systems for nanomedicine*. 15-25

Morozova, S., Alikina, M., Vinogradov, A., & Pagliaro, M. (2020). Silicon Quantum Dots: Synthesis, Encapsulation, and Application in Light-Emitting Diodes. *Frontiers in Chemistry*, *8*(April), 1–8.

Morozova, S., Alikina, M., Vinogradov, A., & Pagliaro, M. (2022). Silicon Quantum Dots: Synthesis, Encapsulation, and Application in Light-Emitting Diodes. *Frontiers in Chemistry*, *8*. 987-991

Mukrimaa, S. S., Nurdyansyah, Fahyuni, E. F., Yulia Citra, A., Schulz, N. D., Ghassan, D., Taniredja, T., Faridli, E. M., & Harmianto, S. (2016). Covariance Structure Analysis of Health-Related Indicators in Home-Dwelling Elderly, Centered on Subjective Health Perception. *Jurnal Penelitian Pendidikan Guru Sekolah Dasar*, 6(August) 26-39.

Na, M., Han, Y., Chen, Y., Ma, S., Liu, J., & Chen, X. (2021). Synthesis of Silicon Nanoparticles Emitting Yellow-Green Fluorescence for Visualization of pH Change and Determination of Intracellular pH of Living Cells. *Analytical Chemistry*, *93*(12), 5185–5193.

© COPYRIGHT UPM

Nishan, U., Ullah, W., Muhammad, N., Asad, M., Afridi, S., Khan, M., Shah, M., Khan, N., & Rahim, A. (2022). Development of a Nonenzymatic Colorimetric Sensor for the Detection of Uric Acid Based on Ionic Liquid-Mediated Nickel Nanostructures. *ACS Omega*, *7*(30), 26983–26991.

Noun, F., Jury, E. A., & Naccache, R. (2021). Elucidating the quenching mechanism in carbon dot-metal interactions–designing sensitive and selective optical probes. *Sensors (Switzerland)*, *21*(4), 1–13.

Orramongkona, P. W., Eeda, K. S., Hansomboon, P. P., Atnarathorn, N. R., Hailapakul, O. C., & Ungchai, W. D. (2018). *A Simple Paper-based Colorimetric Device for Rapid and Sensitive Urinary Oxalate Determinations*. *34*(January).654-659

Pan, C., Qin, X., Lu, M., & Ma, Q. (2022). Water Soluble Silicon Nanoparticles as a Fluorescent Probe for Highly Sensitive Detection of Rutin. *ACS Omega*, *7*(32), 28588–28596.

Peng, F., Su, Y., Zhong, Y., Fan, C., Lee, S. T., & He, Y. (2018). Silicon nanomaterials platform for bioimaging, biosensing, and cancer therapy. *Accounts of Chemical Research*, *47*(2), 612–623.

Pleskacova, A., Brejcha, S., Pacal, L., Kankova, K., & Tomandl, J. (2017). Simultaneous Determination of Uric Acid, Xanthine and Hypoxanthine in Human Plasma and Serum by HPLC–UV: Uric Acid Metabolism Tracking. *Chromatographia*, *80*(4), 529–536.

Ramasami, P., Jhaumeer-Laulloo, S., Rondeau, P., Cadet, F., Seepujak, H., & Seeruttun, A. (2004). Quantification of sugars in soft drinks and fruit juices by density, refractometry, infrared spectroscopy and statistical methods. *South African Journal of Chemistry*, *57*(June 2014), 24–27.

Rambla, F. J., Garrigues, S., & De La Guardia, M. (2023). PLS-NIR determination of total sugar, glucose, fructose and sucrose in aqueous solutions of fruit juices. *Analytica Chimica Acta*, *344*(1–2), 41–53.

Richette, P., Bardin, T., & Médicale, U. F. R. (2010). *Gout*. 13-18

Roychoudhury, A., Francis, A., Patel, J., & Jha, K. (2020). *A decoupler-free simple paper microchip capillary electrophoresis device for simultaneous detection of dopamine , epinephrine and serotonin †*. 25487–25495.

Saidin, N., Idris, N. F., Amaluddin, M. N., Irawati, N., Ralib, A. A. M., & Harun, S. W. (2018). Microfiber-based sensor for measuring uric acid concentrations. *Journal of Telecommunication, Electronic and Computer Engineering*, *10*(2–7), 49–52.

Saqib, M., Qi, L., Hui, P., Nsabimana, A., Halawa, M. I., Zhang, W., & Xu, G. (2018). Development of luminol-N-hydroxyphthalimide chemiluminescence system for highly selective and sensitive detection of superoxide dismutase, uric acid and Co2+. *Biosensors and Bioelectronics*, *99*, 519–524.

© COPYRIGHT UPM

Shen, S., Huang, B., Guo, X., & Wang, H. (2019). A dual-responsive fluorescent sensor for Hg2+ and thiols based on N-doped silicon quantum dots and its application in cell imaging. *Journal of Materials Chemistry B*, *7*(44), 7033–7041.

Shendurse, A. M., & Khedkar, C. D. (2021). Glucose : Properties and analysis. In *Encyclopedia of Food and Health* (1st ed., Issue January). 2675-2688

Shi, W., Ge, B., Jiang, P., Wang, Q., He, L., & Huang, C. (2024). SiQDs-mediated highly efficient hole transfer for photocatalytic overall water splitting over Cu-doped ZnIn2S4. *Applied Catalysis B: Environmental*, *354*(February), 124121.

Sivera, F., Andres, M., & Dalbeth, N. (2022). A glance into the future of gout. *Therapeutic Advances in Musculoskeletal Disease*, *14*, 1–18.

Solanki, H. K., Yadav, O., & Gojiya, A. J. (2021). Relationship between serum uric acid levels and diabetes mellitus: A cross-sectional study. *MedPulse International Journal of Physiology*, *20*(3), 18–21. h

Sun, H., Saeedi, P., Karuranga, S., Pinkepank, M., Ogurtsova, K., Duncan, B. B., Stein, C., Basit, A., Chan, J. C. N., Mbanya, J. C., Pavkov, M. E., Ramachandaran, A., Wild, S. H., James, S., Herman, W. H., Zhang, P., Bommer, C., Kuo, S., Boyko, E. J., & Magliano, D. J. (2022). IDF Diabetes Atlas: Global, regional and country-level diabetes prevalence estimates for 2021 and projections for 2045. *Diabetes Research and Clinical Practice*, *183*, 109119.

Talyzin, I. V., Samsonov, M. V., Samsonov, V. M., Pushkar, M. Y., & Dronnikov, V. V. (2019). Size Dependence of the Melting Point of Silicon Nanoparticles: Molecular Dynamics and Thermodynamic Simulation. *Semiconductors*, *53*(7), 947–953.

Tatli, F., Calam, T. T., Uzun, D., & Hasdemir, E. (2020). The determination of uric acid in the presence of ascorbic acid and dopamine using [(1H-1,2,4-triazole-3-ylimino)methyl]naphthalene-2-ol modified platinum electrode. *Journal of the Faculty of Engineering and Architecture of Gazi University*, *35*(4), 2013–2022.

Terada, S., Xin, Y., & Saitow, K. (2020). *Cost-E ff ective Synthesis of Silicon Quantum Dots*. 342-345

Teymourian, H., Barfidokht, A., & Wang, J. (2020). Electrochemical glucose sensors in diabetes management: An updated review (2010-2020). *Chemical Society Reviews*, *49*(21), 7671–7709.

Tirosh, A., Shai, I., Tekes-Manova, D., Israeli, E., Pereg, D., Shochat, T., Kochba, I., & Rudich, A. (2023). Normal Fasting Plasma Glucose Levels and Type 2 Diabetes in Young Men. *New England Journal of Medicine*, *353*(14), 1454–1462.

Tukimin, N., Abdullah, J., & Sulaiman, Y. (2017). Development of a PrGo-modified electrode for uric acid determination in the presence of ascorbic acid by an electrochemical technique. *Sensors (Switzerland)*, *17*(7).87-91

© COPYRIGHT UPM

Upadhyay, Y., Joshi, R. K., & Sahoo, S. K. (2022). *quantum dots*. 283–304.

Wang, H., & Lee, A. (2015). ScienceDirect Recent developments in blood glucose sensors. *Journal of Food and Drug Analysis*, *23*(2), 191–200.

Wang, X. yan, Zhu, G. bing, Cao, W. di, Liu, Z. jiang, Pan, C. gang, Hu, W. jie, Zhao, W. ying, & Sun, J. fan. (2019). A novel ratiometric fluorescent probe for the detection of uric acid in human blood based on H2O2-mediated fluorescence quenching of gold/silver nanoclusters. *Talanta*, *191*(May 2018), 46–53.

Wang, Y. F., Yu, X., Li, Z., Pan, M. meng, Jiang, M., & Xu, L. (2023). Multicolor fluorescence regulation of N doped silicon quantum dots and the multiple applications. *Sensors and Actuators B: Chemical*, *376*(November 2022).

Wang, Y., Yang, Y., Liu, W., Ding, F., Zhao, Q., Zou, P., Wang, X., & Rao, H. (2018). Colorimetric and fluorometric determination of uric acid based on the use of nitrogen-doped carbon quantum dots and silver triangular nanoprisms. *Microchimica Acta*, *185*(6). 2814-2816

Warner, J. H., Hoshino, A., Yamamoto, K., & Tilley, R. D. (2005). Water-soluble photoluminescent silicon quantum dots. *Angewandte Chemie - International Edition*, *44*(29), 4550–4554.

Wen, Q., Pan, C., Qin, X., Ma, Q., & Feng, S. (2021). One-pot synthesis of novel water-dispersible fluorescent silicon nanoparticles for selective Cr2O72- sensing. *Analytical Methods*, *13*(3), 390–398.

Wen, S., Arakawa, H., & Tamai, I. (2024). Uric acid in health and disease: From physiological functions to pathogenic mechanisms. *Pharmacology and Therapeutics*, *256*, 108615.

Westley, C., Xu, Y., Thilaganathan, B., Carnell, A. J., Turner, N. J., & Goodacre, R. (2017). *Subscriber access provided by UB + Fachbibliothek Chemie | (FU-Bibliothekssystem) Absolute quantification of uric acid in human urine using surface enhanced Raman scattering with the standard addition method*. 1678-1688

Witkowska Nery, E. (2016). *Analysis of Glucose, Cholesterol and Uric Acid*. 453-457

Wu, C., Peng, X., Lu, Q., Li, H., Zhang, Y., & Yao, S. (2018). Ultrasensitive Silicon Nanoparticle Ratiometric Fluorescence Determination of Mercury(II). In *Analytical Letters* (Vol. 51, Issue 7), 823-8239

Wu, J., Dai, J., Shao, Y., & Sun, Y. (2015). One-step synthesis of fluorescent silicon quantum dots (Si-QDs) and their application for cell imaging. *RSC Advances*, *5*(102), 83581–83587.

Xiong, L., Du, X., Kleitz, F., & Qiao, S. Z. (2015). *Cancer-Cell-Specifi c Nuclear-Targeted Drug Delivery by Dual-Ligand-Modifi ed Mesoporous Silica Nanoparticles*. *44*, 5919–5926.

© COPYRIGHT UPM

Xu, G., Zeng, S., Zhang, B., Swihart, M. T., Yong, K. T., & Prasad, P. N. (2016). New Generation Cadmium-Free Quantum Dots for Biophotonics and Nanomedicine. *Chemical Reviews*, *116*(19), 12234–12327.

Xu, X., Ma, S., Xiao, X., Hu, Y., & Zhao, D. (2016). The preparation of high-quality water-soluble silicon quantum dots and their application in the detection of formaldehyde. *RSC Advances*, *6*(101), 98899–98907.

Xuan, T. T., Liu, J. Q., Li, H. L., Sun, H. C., Pan, L. K., Chen, X. H., & Sun, Z. (2014). Microwave synthesis of high luminescent aqueous CdSe/CdS/ZnS quantum dots for crystalline silicon solar cells with enhanced photovoltaic performance. *RSC Advances*, *5*(10), 7673–7678.

Yaacob, A., Ngajikin, N. H., Rashid, N. C. A., Ali, S. H. A., Yaacob, M., Isaak, S., & Cholan, N. A. (2020). Uric acid detection in visible spectrum. *Telkomnika (Telecommunication Computing Electronics and Control)*, *18*(4), 2035–2041.

Yaacob, A., Ngajikin, N. H., Rashid, N. C. A., Yaacob, M., Ali, S. H. A., Azmi, N. E., & Cholan, N. A. (2022). Linearity range enhancement in direct detection of low concentration uric acid. *Optik*, *249*(October 2021), 168243.

Yi, Y., Deng, J., Zhang, Y., Li, H., & Yao, S. (2013). Label-free Si quantum dots as photoluminescence probes for glucose detection. *Chemical Communications*, *49*(6), 612–614.

Yoshimura, M., & Byrappa, K. (2020). Hydrothermal processing of materials: Past, present and future. *Journal of Materials Science*, *43*(7), 2085–2103.

Yu, J., Ge, L., Huang, J., Wang, S., & Ge, S. (2021). Microfluidic paper-based chemiluminescence biosensor for simultaneous determination of glucose and uric acid. *Lab on a Chip*, *11*(7), 1286–1291.

Yu, L., Zhang, S., Xu, H., Wang, L., Zhu, X., Chen, X., Xu, W., Xu, W., Zhang, H., & Lin, Y. (2020). Masking quercetin: A simple strategy for selective detection of rutin by combination of bovine serum albumin and fluorescent silicon nanoparticles. *Analytica Chimica Acta*, *1126*, 7–15.

Zhang, S., & Wang, C. (2023). Precise Analysis of Nanoparticle Size Distribution in TEM Image. *Methods and Protocols*, *6*(4), 1–6.

Zhang, Y., Cai, N., & Chan, V. (2023). Recent Advances in Silicon Quantum Dot-Based Fluorescent Biosensors. *Biosensors*, *13*(3), 311.

Zhang, Y., Chen, S., Yuan, M., Xu, Y., & Xu, H. (2022). Gout and Diet: A Comprehensive Review of Mechanisms and Management. *Nutrients*, *14*(17), 1–22.

Zhang, Y., Guo, S., Huang, H., Mao, G., Ji, X., & He, Z. (2018). Silicon nanodot-based aptasensor for fluorescence turn-on detection of mucin 1 and targeted cancer cell imaging. *Analytica Chimica Acta*, *1035*, 154–160.

© COPYRIGHT UPM

Zhang, Y., Hou, D., Zhao, B., Li, C., Wang, X., Xu, L., & Long, T. (2021). Ratiometric Fluorescence Detection of DNA Based on the Inner Filter Effect of Ru(bpy)2(dppx)2+toward Silicon Nanodots. *ACS Omega*, *6*(1), 857–862.

Zhang, Z., Wei, C., Ma, W., Li, J., & Xiao, X. (2019). *One-Step Hydrothermal Synthesis of Yellow and Green Emitting Silicon Quantum Dots with Synergistic Effect*. 2015-2019

Zhao, X., Meng, X., Ragauskas, A. J., Lai, C., Ling, Z., Huang, C., & Yong, Q. (2022). Unlocking the secret of lignin-enzyme interactions: Recent advances in developing state-of-the-art analytical techniques. *Biotechnology Advances*, *54*(August 2021), 107830.

Zheng, Q., Xiong, L., Yu, L., Wu, D., Yang, C., & Xiao, Y. (2021). An enzyme-free fluorescent sensing platform for the detection of uric acid in human urine. *Journal of Luminescence*, *236*(January), 1–8.

Zhou, J. W., Zheng, X. B., Liu, H. S., Wen, B. Y., Kou, Y. C., Zhang, L., Song, J. J., Zhang, Y. J., & Li, J. F. (2024). Reliable quantitative detection of uric acid in urine by surface-enhanced Raman spectroscopy with endogenous internal standard. *Biosensors and Bioelectronics*, *251*(November 2023), 116101.

Zhou, Y., Qi, M., & Yang, M. (2022). *Spectrochimica Acta Part A : Molecular and Biomolecular Spectroscopy Fluorescence determination of lactate dehydrogenase activity based on silicon quantum dots*. *268*.

Zhou, Z., Shu, T., Sun, Y., Si, H., Peng, P., Su, L., & Zhang, X. (2021). Luminescent wearable biosensors based on gold nanocluster networks for “turn-on” detection of Uric acid, glucose and alcohol in sweat. *Biosensors and Bioelectronics*, *192*(June), 113530-113532

Zur, D., & Des, E. (2008). New Optical Biosensors for Uric Acid and Glucose New Optical Biosensors for Uric Acid and Glucose. *Biosensors*. file:///C:/Carla/Papers/Hydrogels for saccharides/Doktorarbeit.pdf 13-18

© COPYRIGHT UPM

APPENDICES

Appendix 1

Calculations of preparation of Uric acid solution in mole concept.

formula M1V1 = M2V2.

For example, to obtain 0.6mg/ml of uric acid from a stock solution of 0.8mg/ml uric acid solution, it is followed that:

M1 = 0.8mg, V1 =? M2 = 0.6mg and V2 = 10ml

$$V_1 = \frac{0.6 \times 10}{0.8} = 7.5\text{ml}$$

Appendix 2

Fluorescence Intensity of Buffer and Reaction with Silicon Quantum TODs

OPTIMIZATION OF pH BUFFER AT 15 MINUTES 440nm								
pH	Fo	F1	F2	F3	AVE.	Δint	STDV	%STDV
7	66840	49209	47213	49326	48582.67	18257.33	1187.608	2.444509
7.2	69201	48305	44271	43797	45457.67	23743.33	2477.226	5.449523
7.4	69319	46223	47956	46850	47009.67	22309.33	877.4636	1.86656
8	56942	43645	44047	42992	43561.33	13380.67	532.4531	1.222307
8.5	61414	45721	45255	44082	45019.33	16394.67	844.532	1.875932

The same procedure for uric acid optimization of pH

	Effect of reaction of 0.5mg/ml SiQDs with 1mg/ml of glucose solution at 440nm at 15 minutes					
TIME	Fo	F1	F2	F3	AVE.	Δint
0	68414	51048	45621	44157	46942	21472
5	68504	49565	44848	44339	46250.67	22253.33333
10	69201	48305	44271	43797	45457.67	23743.33333
15	68675	47954	43941	43219	45038	23637
20	68196	46255	43912	43533	44566.67	23629.33333
25	67832	47077	43173	43434	44561.33	23270.66667
30	68163	46469	43554	43796	44606.33	23556.66667
35	66641	45985	42622	42826	43811	22830
40	66996	46667	42686	42312	43888.33	23107.66667

The same procedure for uric acid optimization of reaction time

© COPYRIGHT UPM

BIODATA OF STUDENT

Hassan Grema was born in the city of Maiduguri in Borno state, Nigeria. Obtained his National diploma and National Higher Diploma in Ramat Polytechnic and the University of Maiduguri respectively (1992 and 2021). Currently Chief Technologist in the Department of Science Laboratory Technology, Ramat Polytechnic, Maiduguri. The research focus is on the "Non-Enzymatic Fluorescence Sensor Based on Silicon Quantum Dots for the Detection of Uric Acid and Glucose"

© COPYRIGHT UPM

LIST OF PUBLICATIONS

Hassan Grema, Jaafar Abdullah, Nor Azah Yusof . (2024). Characterization of Silicon Quantum Dots Synthesized Via Hydrothermal Method and Its Application for Glucose Detection (Pencirian Titik Kuantum Silikon Sintesis Melalui Kaedah Hidroterma dan Penggunaannya. *28*(6), 1417–1427.

© COPYRIGHT UPM

© COPYRIGHT UPM